

Achieving Optimal-Distance Atom-Loss Correction via Pauli Envelope

Pengyu Liu,^{1,2} Shi Jie Samuel Tan,^{1,3} Eric Huang,^{1,3} Umut A. Acar,² Hengyun Zhou,¹ and Chen Zhao^{1,*}

¹*QuEra Computing*

²*Carnegie Mellon University*

³*Joint Center for Quantum Information and Computer Science,
NIST/University of Maryland, College Park, Maryland 20742, USA.*

Atom loss is a major error source in neutral-atom quantum computers, accounting for over 40% of the total physical errors in recent experiments. Unlike Pauli errors, atom loss poses significant challenges for both syndrome extraction and decoding due to its nonlinearity and correlated nature. Current syndrome extraction circuits either require additional physical overhead or do not provide optimal loss tolerance. On the decoding side, existing methods are either computationally inefficient, achieve suboptimal logical error rates, or rely on machine learning without provable guarantees. To address these challenges, we propose the *Pauli Envelope* framework, which generalizes existing loss-to-Pauli approximations and enables rigorous analysis. This framework constructs a Pauli envelope that bounds the effect of atom loss while remaining low weight and efficiently computable. Guided by this framework, we first design a new atom-replenishing syndrome extraction circuit, the *Mid-SWAP syndrome extraction*, that reduces error propagation with no additional space-time cost. We then propose an optimal decoder for Mid-SWAP syndrome extraction: the *Envelope-MLE decoder* formulated as a Mixed-Integer Linear Program (MILP) that achieves optimal effective code distance $d_{\text{loss}} \sim d$ for atom-loss errors. Inspired by the exclusivity constraint of the optimal decoder, we also propose an *Envelope-Matching decoder* to approximately enforce the exclusivity constraint within the Minimum-Weight Perfect Matching (MWPM) framework. This decoder achieves $d_{\text{loss}} \sim 2d/3$, surpassing the previous best algorithmic decoder, which achieves $d_{\text{loss}} \sim d/2$ even with an MILP formulation. Combined with recent fast correlated-decoding techniques, our method enables efficient, high-threshold loss decoding for transversal surface-code logical circuits using MWPM. Circuit-level simulations demonstrate that our approach attains up to 40% higher thresholds and 30% higher effective distances compared with existing algorithmic decoders and syndrome extraction circuits in the loss-dominated regime. On recent experimental data, our Envelope-MLE decoder improves the error suppression factor of a hybrid MLE-machine-learning decoder from $\Lambda = 2.14$ to $\Lambda = 2.24$.

I. INTRODUCTION

Quantum computing promises transformative advances in cryptography [1], materials science [2], and optimization [3], yet realizing this potential requires fault-tolerant operation through quantum error correction [4]. The most widely studied quantum error-correcting code for achieving fault tolerance is the surface code [5, 6]. It is known to possess a high physical error threshold under various noise models [7, 8] and can be implemented with nearest-neighbor connectivity. Among the leading platforms for fault-tolerant quantum computing, neutral-atom quantum computers have demonstrated exceptional scalability and gate fidelity [9–13]. However, atom loss remains one of the key challenges for achieving fault tolerance in these systems, accounting for more than 40% of the total physical errors in recent experiments [10].

When an atom is lost, any subsequent gates involving that atom are effectively deleted from the circuit, leading to correlated Clifford errors that propagate through the computation [14–16]. This error mechanism exhibits two features that make it particularly challenging. First, atom loss persists until replenishment, causing errors to

accumulate across multiple gates and even multiple syndrome extraction rounds. Specialized syndrome extraction circuits are therefore needed to localize loss effects in both time and space. Second, unlike Pauli errors, which propagate and combine linearly, atom loss behaves nonlinearly. Multiple atom losses may produce detector patterns that cannot be derived by composing individual loss patterns, posing significant challenges for decoder design and analysis. To address these challenges, we develop the *Pauli Envelope* framework to linearize the nonlinear loss effects into tractable Pauli errors. This framework rigorously characterizes how atom loss effects can be bounded by low-weight Pauli errors, guiding the design of syndrome extraction circuits and decoding algorithms with provable performance guarantees. Unlike prior heuristic approximations, the Pauli envelope provides two key guarantees: (1) *correctness*: if the Pauli envelope is decoded correctly, the original atom-loss events are guaranteed to be decoded correctly; and (2) *low weight*: the Pauli envelope has low weight for loss errors, leading to stronger distance guarantees.

Guided by this framework, we make the following contributions:

(1) Syndrome extraction circuit: We introduce the *Mid-SWAP syndrome extraction*, which reduces the propagation of loss effects with no additional space-time overhead compared to the conventional surface code syn-

* czhao@quera.com

drome extraction circuit. This circuit can correct up to $\sim d$ loss errors (we use $\sim d$ to denote $d \pm O(1)$), which is optimal for a distance- d surface code and significantly outperforms the SWAP syndrome extraction of [14], which fails to correct $\sim d/2$ loss errors.

(2) Optimal-distance decoder: We propose the *Envelope-Most-Likely-Error decoder (Envelope-MLE decoder)*, which correctly decodes up to $\sim d$ loss errors for the Mid-SWAP syndrome extraction. This significantly outperforms the *Average-MLE decoder* of [14], which fails to correct $\sim d/2$ loss errors. The key insight is that each atom loss triggers exactly one detector pattern in our Pauli envelope formulation, imposing an *exclusivity* constraint that the Average-MLE decoder fails to enforce.

(3) Efficient decoder: Inspired by the exclusivity constraint, we design the *Envelope-Matching decoder* for efficient decoding. Instead of changing edge weights to a constant, which becomes negligible compared with Pauli error weights when $p_{\text{pauli}} \rightarrow 0$, as done in the *Marginal-Matching decoder* by Gu et al. [17, 18], we rescale the affected edge weights by a constant factor to discourage selecting multiple edges in the same envelope, approximately enforcing the exclusivity constraint. This decoder corrects up to $\sim 2d/3$ loss errors for the Mid-SWAP syndrome extraction, outperforming the $\sim d/2$ loss errors of the Marginal-Matching decoder. As an MWPM-based decoder, the Envelope-Matching decoder naturally integrates with fast correlated decoding techniques for transversal logical circuits [19–21].

Eff. Dist. \ Decoder	Circuit	SWAP Mid-SWAP Teleportation		
		SWAP	Mid-SWAP	Teleportation
Vanilla Matching		$d/3$	$d/3$	$d/3$
Average-MLE [14]		$d/2$	$d/2$	$d/2$
Marginal-Matching [17, 18]		$d/2$	$d/2$	$d/2$
Envelope-MLE		$d/2$	d	d
Envelope-Matching		$d/2$	$2d/3$	$2d/3$
Space-Time Cost		$1\times$	$1\times$	$\geq 2\times$

TABLE I: Theoretical performance comparison of decoders and syndrome extraction circuits with atom-loss replenishment. The bold entries are introduced in this paper. All distances are up to additive constants. Teleportation-based syndrome extraction is briefly discussed in Appendix H.

Table I summarizes the theoretical performance of our proposed decoders (Envelope-MLE decoder and Envelope-Matching decoder) compared to existing approaches across several syndrome extraction circuits with atom-loss replenishment, including our newly proposed Mid-SWAP syndrome extraction.

We evaluate the performance of our proposed decoders and syndrome extraction circuit using a circuit-level noise model. In the loss-dominated regime, our approach achieves up to 40% higher thresholds and 30% higher effective distances than prior approaches.

This paper is organized as follows: Section II reviews the atom-loss error model and essential background for quantum error correction. Section III introduces the Pauli envelope framework. Section IV presents the Mid-SWAP syndrome extraction circuit. Section V describes the Envelope-MLE decoder. Section VI presents the Envelope-Matching decoder. Section VII provides numerical evaluation.

II. ATOM LOSS

Various terms are used in the literature to describe errors where qubits leave the computational subspace [22–24]. In this paper, we characterize these errors based on two criteria: the timing of error detection and the impact on subsequent gates. As summarized in Table II, we define atom loss as an error where detection is delayed until measurement, causing any subsequent gates involving the lost qubits to be effectively removed. And we use the term *erasure errors* as those where detection is instantaneous, resulting in subsequent gates becoming maximum depolarizing errors.

TABLE II: Comparison of erasure errors and atom loss.

	Erasure Error	Atom Loss
Detection timing	Instantaneous	Upon measurement
Effects	Maximum depolarizing	Gate-removing
Distance	d	$\sim d$

In the minimal hardware model we adopt, all atoms are discarded after measurement, and replenishment is performed solely by preparing fresh ancillas initialized in $|0\rangle$. This model is compatible with current neutral-atom platforms and represents the least demanding setting capable of fault-tolerant quantum computation [9]. We assume this model throughout this paper. To enable fault-tolerant quantum computation, we need specialized syndrome extraction circuits that replenish lost atoms, including data qubits.

Recent experiments have demonstrated state-selective readout [9, 10], which can be viewed as a three-outcome measurement that distinguishes whether the qubit is in state $|0\rangle$, state $|1\rangle$, or the atom has been lost. However, this readout is destructive and thus cannot be applied mid-circuit without destroying the quantum state when the atom is present. Consequently, when an atom loss is detected, we only learn that the loss occurred at some point between the last reset and the measurement, without knowing exactly when.

Despite these difficulties, our results demonstrate that atom loss has the same effective distance as erasure errors, contrary to the previous belief that atom loss reduces effective distance compared to erasure errors [14, 25].

To analyze how loss impacts syndrome extraction and decoding, we model atom loss as a gate-removing error following [14]: after an atom is lost, all subsequent gates acting on that atom (including single-qubit and two-qubit gates) are removed, as illustrated in Fig. 1.

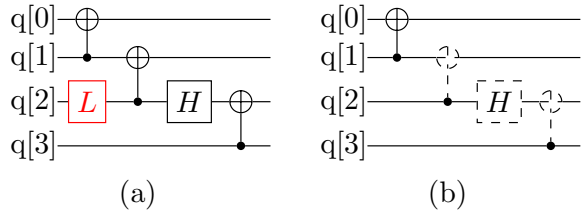


FIG. 1: Atom loss as a gate-removing error. (a) An atom loss occurs at the beginning of the circuit on qubit $q[2]$. (b) The atom loss removes all subsequent gates acting on qubit $q[2]$.

Decoding relies on the concept of *detectors*. Detectors are linear combinations of measurements that are deterministic under ideal execution of a Clifford circuit. For example, in a surface code quantum memory, a detector is typically the XOR of two consecutive syndrome measurements at the same stabilizer location: under ideal execution, both measurements yield the same result, so their XOR is always 0. During noisy execution, we obtain a detector pattern \mathcal{D} , indicating the set of detectors that are different from the ideal outcome, and a decoder finds an error configuration that can explain this pattern.

A *detector error model* (DEM) is a collection of elementary error mechanisms, each with an associated probability of occurrence and the detector pattern it triggers. For Pauli noise in Clifford circuits, errors compose linearly: the combined detector pattern of multiple Pauli errors is the sum (modulo 2) of their individual detector patterns, which enables a compact DEM description.

Atom loss breaks this additivity because it introduces Clifford errors. The interactions between Clifford errors are much more complicated than those of Pauli errors. As a result, the detector pattern resulting from multiple loss events generally cannot be obtained by summing the detector patterns of individual loss events in isolation.

Fig. 2 shows a minimal example: without error, or losing either the first or the second atom alone, the final qubit yields $|1\rangle$ in panels (a)–(c), while with both losses it yields $|0\rangle$ in panel (d).

This nonlinearity poses a significant challenge for decoding: even if we know exactly which atoms were lost and when, we do not have a simple closed-form expression for the distribution of measurement outcomes, as we do for Pauli errors. This makes rigorous analysis of atom-loss decoding performance challenging.

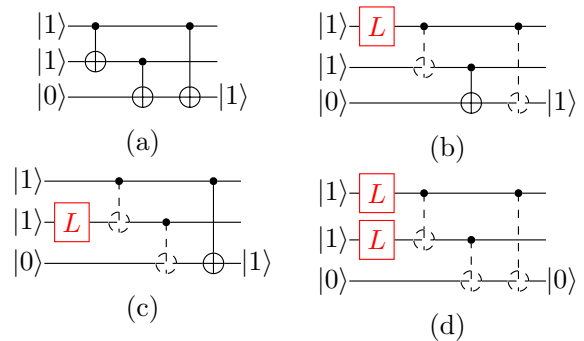


FIG. 2: The composition of atom loss is nonlinear.

III. PAULI ENVELOPE

In this section, we formalize the Pauli envelope, prove its key properties, and show how to construct Pauli envelopes for atom loss.

A. Formalization of Pauli Envelope

The key idea behind the Pauli envelope is simple: although atom loss behaves nonlinearly, its effect on the decoder can be *bounded* by a set of Pauli errors. If a decoder can correctly handle all errors in this bounding set, it will also correctly decode the original atom loss. This reduces the complex problem of decoding atom loss to the well-understood problem of decoding Pauli errors.

We now formalize this intuition. Consider a Clifford circuit \mathcal{C} with Pauli error configuration p and loss configuration l , where a *configuration* is a subset of space-time locations at which the error or loss occurs. If an atom is lost more than once in a configuration, we ignore subsequent loss events.

Let $(\mathcal{D}(p, l), \mathcal{O}(p, l))$ denote the detector-observable pair produced by running \mathcal{C} with error p and loss l [26]. Define $\mathcal{S}(p, l) = \{(\mathcal{D}(p, l), \mathcal{O}(p, l))\}$ as the set of possible outcomes, and extend this to sets of configurations: $\mathcal{S}(P, L) = \{(\mathcal{D}(p, l), \mathcal{O}(p, l)) \mid p \in P, l \in L\}$.

Let \mathcal{R} denote the *loss-resolving readout* function that maps loss configurations to loss-resolving readouts. Multiple loss configurations may produce the same loss-resolving readout, so we define $\mathcal{L}(r) = \{l : \mathcal{R}(l) = r\}$ as the preimage.

Definition 1 (Pauli Envelope). *A loss configuration l has Pauli envelope E , where E is a set of Pauli error configurations, if for all Pauli error configurations p ,*

$$\mathcal{S}(p, l) \subseteq \mathcal{S}(p \oplus E, \emptyset),$$

where \emptyset denotes no atom loss and $p \oplus E$ denotes the composition of p with errors from E , i.e., $p \oplus E = \{p \oplus e : e \in E\}$.

Similarly, we say a readout r has Pauli envelope E if $\mathcal{S}(p, \mathcal{L}(r)) \subseteq \mathcal{S}(p \oplus E, \emptyset)$ for all p .

In other words, any detector-observable pair that can arise from a Pauli error p combined with any loss configuration producing readout r can also arise from the Pauli errors $p \oplus E$ with no atom loss.

The Pauli envelope ensures that if we can correctly decode the Pauli envelope, we can decode the atom losses correctly.

Lemma 1 (Sufficiency of Decoding Pauli Envelope). *Let \mathcal{C} be a Clifford circuit suffering from a Pauli error configuration p and a loss configuration with readout r . Suppose that r has Pauli envelope E . Let Dec be a deterministic decoder that maps detector patterns and loss-resolving readouts to logical observable predictions.*

If $\text{Dec}(\cdot, r)$ correctly decodes all detector-observable pairs in $\mathcal{S}(p \oplus E, \emptyset)$, i.e., for all $(\mathcal{D}, \mathcal{O}) \in \mathcal{S}(p \oplus E, \emptyset)$, we have $\text{Dec}(\mathcal{D}, r) = \mathcal{O}$, then $\text{Dec}(\cdot, r)$ also correctly decodes all detector-observable pairs in $\mathcal{S}(p, \mathcal{L}(r))$.

Proof. Since r has Pauli envelope E , by definition we have

$$\mathcal{S}(p, \mathcal{L}(r)) \subseteq \mathcal{S}(p \oplus E, \emptyset).$$

Therefore, if $\text{Dec}(\cdot, r)$ correctly decodes all pairs in $\mathcal{S}(p \oplus E, \emptyset)$, it also correctly decodes all pairs in $\mathcal{S}(p, \mathcal{L}(r))$. \square

Next, we relate the logical error rate with atom loss to the failure probability with the Pauli envelope. We first extend the definition of logical error rate to include atom loss.

Definition 2 (Logical Error Rate with Atom Loss). *Let \mathcal{C} be a Clifford circuit with the following error model:*

- Pauli error configurations are sampled from distribution \mathcal{P}_p .
- Loss configurations are sampled from distribution \mathcal{P}_l .

The logical error rate $P_{\text{LER}}(\mathcal{C}, \mathcal{P}_l, \mathcal{P}_p, \text{Dec})$ is defined as

$$P_{\text{LER}} = \Pr_{\substack{l \sim \mathcal{P}_l \\ p \sim \mathcal{P}_p}} [\text{Dec}(\mathcal{D}(p, l), \mathcal{R}(l)) \neq \mathcal{O}(p, l)] \quad (1)$$

We further define the failure probability with Pauli envelope.

Definition 3 (Failure Probability with Pauli Envelope). *Let \mathcal{C} be a Clifford circuit with the following error model:*

- Pauli error configurations are sampled from distribution \mathcal{P}_p .
- Loss configurations are sampled from distribution \mathcal{P}_l . However, this loss configuration is not applied directly to the circuit. Instead, we compute the loss-resolving readout $r = \mathcal{R}(l)$ and find the corresponding Pauli envelope $E(r)$.

The failure probability $P_{\text{fail}}(\mathcal{C}, \mathcal{P}_l, \mathcal{P}_p, \text{Dec})$ is defined as

$$P_{\text{fail}} = \Pr_{\substack{l \sim \mathcal{P}_l \\ p \sim \mathcal{P}_p}} [\exists (\mathcal{D}, \mathcal{O}) \in \mathcal{S}(p \oplus E(r), \emptyset) : \text{Dec}(\mathcal{D}, r) \neq \mathcal{O}]. \quad (2)$$

Notice that the failure probability does not average over $E(r)$, but counts the entire $E(r)$ as a failure if any error in $E(r)$ causes a decoding failure.

Theorem 1 (Logical Error Rate is Upper-Bounded by Failure Probability).

$$P_{\text{LER}}(\mathcal{C}, \mathcal{P}_l, \mathcal{P}_p, \text{Dec}) \leq P_{\text{fail}}(\mathcal{C}, \mathcal{P}_l, \mathcal{P}_p, \text{Dec}).$$

Proof. See [Appendix A 1](#). \square

The key insight is that by [Lemma 1](#), any decoding failure with loss can be traced back to a failure in decoding the Pauli envelope $p \oplus E$ without loss. This establishes that the logical error rate is bounded by the failure probability of decoding the envelope errors.

B. Construction of Pauli Envelope for Atom Loss

The preceding results show that all performance guarantees for the Pauli envelope will automatically transfer to atom loss errors. A natural question arises: can we construct a Pauli envelope with good decoding properties, specifically one that is linear and low-weight? We show below that the answer is affirmative.

Without loss of generality, assume \mathcal{C} is generated by CZ , H , and S gates. For a loss configuration containing a single atom loss location, the Pauli envelope E can be constructed as follows.

Lemma 2 (Pauli Envelope of Atom Loss). *Let \mathcal{C} be a Clifford circuit and l be an atom loss configuration corresponding to a single atom loss location. Then the following construction yields a Pauli envelope E for l .*

Let $L_i = \{I, X, Y, Z\}$ denote the set of all single-qubit Pauli operators at a specific space-time location i . For two such sets, we define $L_i \oplus L_j = \{e_i \oplus e_j : e_i \in L_i, e_j \in L_j\}$ as the set of all pairwise compositions. We identify the relevant locations: (1) the loss location itself, (2) immediately after each subsequent Hadamard gate acting on the lost atom, and (3) just before measuring the lost atom. The Pauli envelope is then $E = L_1 \oplus L_2 \oplus \dots \oplus L_k$, where L_1, \dots, L_k are the Pauli sets at these relevant locations.

Proof. See [Appendix A 2](#). \square

The key insight of the proof is that a lost atom can be modeled as if reset gates are inserted after each gate following the loss event. Since CZ and S gates preserve $|0\rangle$, redundant resets between consecutive CZ and S gates are not required.

This construction ensures several key linearity properties:

Lemma 3 (Linearity of Pauli Envelope). (a) Consider a loss configuration $l = l_1 \oplus l_2 \oplus \dots \oplus l_k$, where each l_i is a single-atom loss configuration. The following composition yields a Pauli envelope for l : $E(l) = \bigoplus_{i=1}^k E(l_i)$.

(b) For a readout r corresponding to a single atom loss with multiple possible loss configurations $\mathcal{L}(r) = \{l^{(1)}, l^{(2)}, \dots\}$, the following union yields a Pauli envelope for r : $E(r) = \bigcup_{l \in \mathcal{L}(r)} E(l)$.

(c) For a readout $r = r_1 \oplus r_2 \oplus \dots \oplus r_m$, where each r_i is a single-atom loss readout corresponding to m atom losses, the following composition yields a Pauli envelope for r : $E(r) = \bigoplus_{i=1}^m E(r_i)$.

Proof. See Appendix A 3. \square

This linearity ensures that the Pauli envelope for any combination of atom losses can be constructed from single-atom-loss envelopes, avoiding the need to analyze exponentially many multi-loss scenarios directly or to reason about the nonlinearity of atom loss.

In the following, we mainly use *CNOT* circuits for simplicity. To apply the results to *CNOT* circuits, we can view each *CNOT* as compiled into *CZ* and *H* gates. Thus, we need to add Pauli errors whenever a qubit changes its role from a target qubit to a control qubit or vice versa.

We explicitly construct the Pauli envelope for an ancilla atom loss in a standard surface code syndrome extraction circuit.

Example 1 (Ancilla qubit loss). *Fig. 3 illustrates part of a syndrome extraction circuit with an ancilla qubit loss. When the final readout r reveals that the ancilla qubit is lost, the corresponding Pauli envelope is*

$$E = (L_1 \oplus L_5) \cup (L_2 \oplus L_5) \cup (L_3 \oplus L_5) \cup (L_4 \oplus L_5) \cup L_5.$$

Each L_i denotes the set $\{I, X, Y, Z\}$ occurring at different locations as illustrated in Fig. 3.

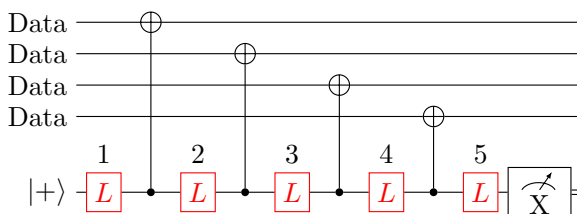


FIG. 3: Surface code syndrome extraction circuit with an ancilla-qubit loss.

IV. LOSS-REPLENISHING SYNDROME EXTRACTION FOR SURFACE CODES

As discussed in Section II, specialized syndrome extraction circuits are needed to localize the effects of atom

loss in both time and space while satisfying hardware restrictions. In particular, loss-resolving readout can only be applied during measurement, which inevitably collapses the logical information.

In this section, we review the SWAP syndrome extraction, proposed by [27, 28] and adopted by [14, 29, 30], which handles atom loss under these constraints. We then use the Pauli envelope framework to analyze its limitations and introduce a new syndrome extraction circuit, the Mid-SWAP syndrome extraction, which doubles the effective distance against atom loss compared to the SWAP syndrome extraction without additional hardware overhead.

A. SWAP Syndrome Extraction

The SWAP syndrome extraction addresses atom loss on data qubits by exchanging the roles of ancilla and data qubits after each syndrome extraction round. As shown in Fig. 4, the final *CNOT* interactions (ticks 4 and 8) are reversed, followed by atom shuttling. After the measurements, a classically controlled Pauli gate is applied to the data qubit, which can be implemented in software. This ensures that each atom is measured and replenished within 8 *CNOT* gates after initialization.

During the data phase (the last 4 ticks), the *CNOT* direction alternates between control and target. According to Lemma 2, regardless of whether the atom loss occurs during or before the data phase, there will always be data errors on the data qubits.

Furthermore, if atom loss occurs during the ancilla phase, it will create a hook error originating from the ancilla qubit because a Pauli error needs to be inserted at the position of the loss.

Fig. 5 summarizes this observation about the life cycle: an atom loss early in the ancilla phase of the SWAP syndrome extraction leads to **both a hook error and a data error** in the syndrome extraction circuit, making it less robust against atom loss.

In Appendix B 2, we formally show that this widespread error limits the SWAP syndrome extraction to $d_{\text{loss}} \sim d/2$.

B. Mid-SWAP Syndrome Extraction

To address the possibility of creating both a hook error and a data error from a single atom loss event in the SWAP syndrome extraction, we introduce the Mid-SWAP syndrome extraction, which performs atom shuttling during each syndrome extraction round rather than at the end of each round. This allows each newly replenished atom to serve as a data qubit first and then transition to an ancilla qubit.

As illustrated in Fig. 6, the Mid-SWAP syndrome extraction modifies a standard surface code syndrome extraction circuit by inserting an atom-shuttling step im-

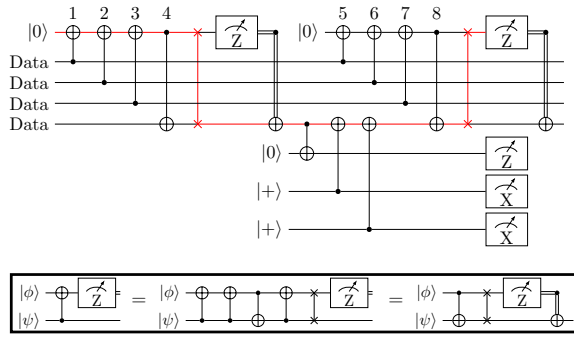


FIG. 4: Circuit for SWAP syndrome extraction, showing two consecutive rounds. $CNOT$ gates involving other qubits are omitted for brevity. The red line indicates the life cycle of a physical atom, and the $SWAP$ gate indicates atom shuttling. The correctness of this circuit is shown by the circuit identity below.

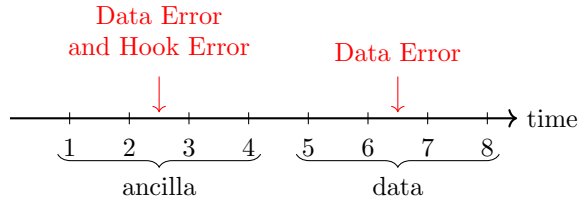


FIG. 5: Timeline of an atom in the SWAP syndrome extraction. The ticks correspond to the gate labels in Fig. 4. The red arrow marks an atom loss between ticks 2 and 3.

mediately after the first $CNOT$ gate in each round, while all other $CNOT$ gates remain unchanged.

Fig. 7 shows the life cycle of a qubit in the Mid-SWAP syndrome extraction.

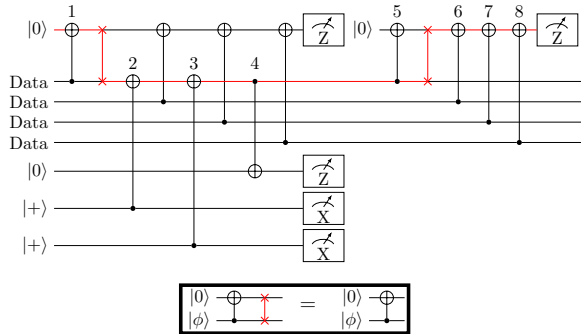


FIG. 6: Circuit for Mid-SWAP syndrome extraction, showing two consecutive syndrome extraction rounds. The correctness of this circuit is shown by the circuit identity below.

If an atom loss occurs during the data phase, it will cause a data error on that data qubit but will not create hook errors during the ancilla phase because the entire

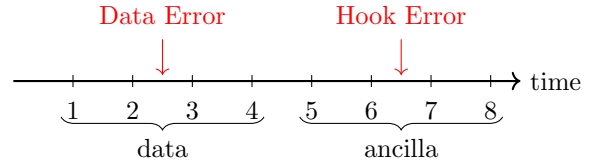


FIG. 7: Timeline of an atom in the Mid-SWAP syndrome extraction. The ticks correspond to the gate labels in Fig. 6.

ancilla phase is skipped. Moreover, because an ancilla qubit is always a target or always a control of the $CNOT$ gates, Lemma 2 implies that there is no need to insert any Pauli error on the ancilla if it is lost before the beginning of the ancilla phase, except for a possible measurement error.

If an atom loss occurs during the ancilla phase, it will cause a hook error but not a data error because only gates after the loss are affected.

This ensures that in Mid-SWAP syndrome extraction, an atom loss can only cause **either a hook error or a data error**, but not both. Lemma 4 formalizes this observation. Focusing on physical Z errors detected by X -stabilizer measurements and projecting each detector onto the X - Y plane, a Z -ancilla loss in the Mid-SWAP syndrome extraction triggers at most one edge forming a Z -shaped path as illustrated by S_1 , S_2 , and S_3 in Fig. 8, while an X -ancilla loss triggers at most one edge at a fixed position. This structure is crucial for the decoder analysis in the following sections. After introducing the Envelope-MLE decoder in the next section, we prove the optimality of Mid-SWAP syndrome extraction.

Lemma 4 (Exclusive Loss-induced Patterns in Mid-SWAP syndrome extraction). *Consider a standard surface code with data qubits and ancilla qubits mapped to the grid as shown in Fig. 8. Assume the logical Z observable is defined horizontally, and stabilizers are extracted in the order shown above the figure. We focus on logical Z errors; logical X errors can be handled symmetrically.*

In the matching graph for logical Z decoding, only X -stabilizer measurements (which detect Z -type data errors) are relevant. There are two types of ancilla loss events to consider: loss at a Z -stabilizer ancilla position and loss at an X -stabilizer ancilla position.

For a Z -stabilizer ancilla loss detected at position (x, y) , the loss triggers at most one of the following Z -error detector pairs (projected onto the (x, y) plane), which together form a Z -shaped path:

1. $S_1 = ((x - 2, y), (x, y + 2))$: a diagonal edge from left to top.
2. $S_2 = ((x, y + 2), (x, y - 2))$: a vertical edge from top to bottom.
3. $S_3 = ((x, y - 2), (x + 2, y))$: a diagonal edge from bottom to right, parallel to S_1 .

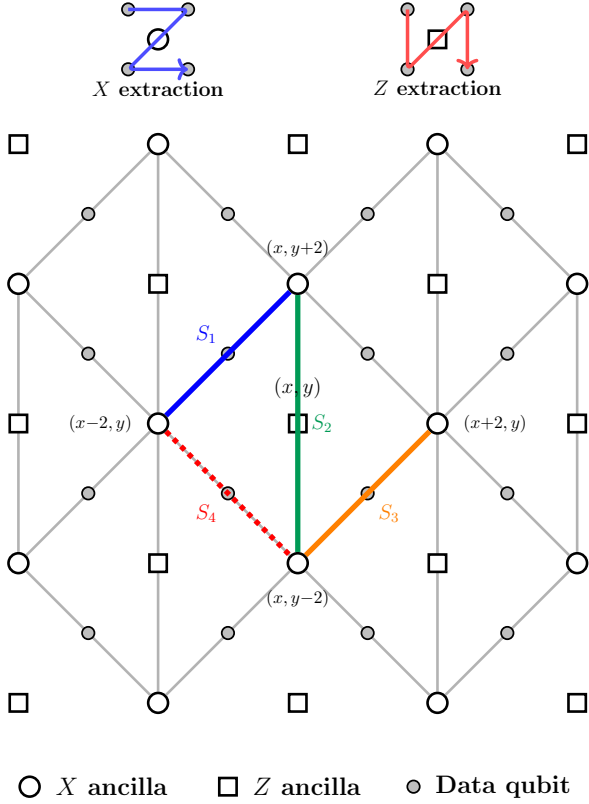


FIG. 8: Detector patterns induced by a single atom loss in the Mid-SWAP syndrome extraction. Each edge represents an error mechanism that can trigger the two endpoint detectors. X -detectors correspond to X stabilizers and are triggered by Z errors; similarly, Z -detectors correspond to Z stabilizers and are triggered by X errors. An atom loss detected at position (x, y) (during Z -ancilla measurements) triggers at most one of three detector pairs: S_1 , S_2 , and S_3 , which together form a Z -shaped path in the matching graph. An atom loss detected at position $(x, y - 2)$ (during X -ancilla measurements) can only trigger S_4 .

For an X -stabilizer ancilla loss detected at position $(x, y - 2)$, the loss triggers $S_4 = ((x - 2, y), (x, y - 2))$ or none of these detector pairs.

Proof. This follows from enumerating all possible errors; details are provided in [Appendix B 1](#). \square

V. ENVELOPE-MLE DECODER

We introduce the Envelope-MLE decoder, formulated as a Mixed-Integer Linear Program (MILP), which jointly optimizes over Pauli envelope selections and Pauli errors to find a minimum-weight error configuration consistent with the observed detector outcomes. Throughout this section, we assume loss-resolving readouts are perfect; extensions to noisy readouts are discussed in [Ap-](#)

[pendix C 5](#).

Algorithm 1 (Envelope-MLE decoder). Before receiving the detector patterns and loss-resolving readouts, the decoder first performs the following steps as preprocessing:

1. **Find the Pauli envelope for each loss-resolving readout:** For each loss-resolving readout r_m corresponding to a single atom loss, find its Pauli envelope E_m according to [Lemma 2](#).
2. **Assign variables for loss patterns:** For each pair $(\mathcal{D}_{m,j}, \mathcal{O}_{m,j}) \in \mathcal{S}(E_m, \emptyset)$, assign a binary variable $x_{m,j} \in \{0, 1\}$, indicating whether the loss pattern is selected ($x_{m,j} = 1$) or not ($x_{m,j} = 0$). Here, the index m represents the loss-resolving readout index, while j represents the index of elements of the Pauli envelope.
3. **Assign variables for Pauli errors:** For each Pauli error mechanism i in the circuit, assign a binary variable $y_i \in \{0, 1\}$, indicating whether the Pauli error mechanism is selected ($y_i = 1$) or not ($y_i = 0$).

After receiving the detector patterns, the decoder performs the following steps:

1. **Enforce constraints:**

(i) **Detector satisfaction:** For each detector d , enforce

$$\sum_i D_{i,d} y_i + \sum_{m,j} D_{m,j,d} x_{m,j} \equiv s_d \pmod{2}, \quad (3)$$

where $D_{i,d} \in \{0, 1\}$ indicates whether Pauli error i flips detector d , $D_{m,j,d} \in \{0, 1\}$ indicates whether loss pattern (m, j) flips detector d , and $s_d \in \{0, 1\}$ is the observed value of detector d .

(ii) **Loss exclusivity:** For each loss-resolving readout r_m , where $r_m = 1$ indicates the m -th atom is lost, enforce

$$\sum_j x_{m,j} = r_m, \quad (4)$$

ensuring exactly one detector pattern is selected per loss event.

2. **Minimize Pauli error weight:** Subject to the above constraints, solve the following MILP:

$$\min_{x,y} \sum_i w_i y_i \quad (5)$$

where $w_i = -\log \frac{p_i}{1-p_i}$ is the log-likelihood ratio of Pauli error i .

3. **Predict logical observable:** Let $x_{m,j}^*, y_i^*$ be the optimal solutions to the MILP. Calculate the predicted logical flip:

$$\mathcal{O}_{pred} = \bigoplus_i y_i^* \mathcal{O}_i \oplus \bigoplus_{m,j} x_{m,j}^* \mathcal{O}_{m,j} \quad (6)$$

where \mathcal{O}_i is the observable flip caused by Pauli error i .

Lemma 5 (Optimality of Envelope-MLE decoder). *The Envelope-MLE decoder finds a solution with Pauli weight no greater than that of the actual error configuration.*

Proof. See [Appendix C 1](#). \square

The optimality follows from observing that by [Lemma 2](#), the actual error configuration is always feasible for the MILP. We now show the decoder performance on the Mid-SWAP syndrome extraction, where the localized Pauli envelope structure enables stronger guarantees.

From now on, we assume all w_i are equal to a constant w .

Theorem 2 (MLE Decoder Achieves Optimal Distance). *The Envelope-MLE decoder achieves optimal distance for the Mid-SWAP syndrome extraction. Specifically, the decoder correctly decodes whenever*

$$n_l + 2n_p < d, \quad (7)$$

where n_l is the number of atom losses, n_p is the number of Pauli errors, and d is the code distance.

Proof. See [Appendix C 3](#). \square

The proof analyzes the symmetric difference between the actual error and decoder output. By the optimality of the MLE decoder, the Pauli component has weight at most $2n_p w$. Forming an undetectable logical error with n_l loss pattern mismatches requires Pauli weight at least $(d - n_l)w$. Combining these bounds yields the condition $2n_p + n_l \geq d$ for decoder failure.

This bound is tight. When $n_l + 2n_p = d$, consider a length- d logical X string. Suppose the first n_l data qubits on the string are lost, so the remaining segment has length $d - n_l = 2n_p$. Now compare two fault patterns: (i) apply the logical X and add X errors on any n_p of the remaining qubits; (ii) apply no logical operator and instead add X errors on the complementary n_p remaining qubits. After tracing out the lost qubits, the two cases yield the same physical state and identical loss-resolving readouts, so a decoder cannot distinguish them and must fail on at least one, inducing a logical error.

[Theorem 2](#) by itself does not guarantee fault tolerance. We extend the threshold theorem to include atom loss, showing that the logical error rate can be made arbitrarily small by increasing the code distance.

Theorem 3 (Failure Probability Threshold). *For the Mid-SWAP syndrome extraction with code distance d , subject to independent atom loss with rate p_{loss} and background Pauli errors with rate p_{pauli} , the failure probability of the Envelope-MLE decoder satisfies:*

$$P_{\text{fail}} = O\left(p_{\text{th}}^{-d} (p_{\text{loss}}^{d_{\text{loss}}} + p_{\text{pauli}}^{d_{\text{pauli}}})\right),$$

where $d_{\text{loss}} \sim d$ and $d_{\text{pauli}} \sim d/2$.

Note that this threshold p_{th} differs from the standard threshold for Pauli-only errors, but it should be a constant independent of the code distance d and the physical error rates p_{loss} and p_{pauli} to ensure the logical error rate is exponentially suppressed as the code distance increases. We define it this way to let the atom loss and Pauli errors share a single threshold. [\[31\]](#)

Proof. See [Appendix C 4](#). \square

The proof follows from standard lattice counting arguments. By defining $p := \max(p_{\text{loss}}, \sqrt{p_{\text{pauli}}})$, we unify the error rates and show the sum is dominated by minimum-weight configurations, yielding the stated scaling.

In contrast, the Average-MLE decoder proposed in [\[14\]](#) constructs a detector error model by enumerating all possible detector patterns induced by individual atom losses and combining them with the Pauli detector error model as if all errors are independent. We attribute its suboptimal performance to two limitations that our Envelope-MLE decoder avoids:

- **No exclusivity constraint:** The Average-MLE decoder does not enforce that each atom can be lost at most once. As a result, certain detector patterns caused by Pauli errors may be incorrectly explained as loss errors, even when no actual loss configuration can produce them. This miscorrection limits the decoder to $d_{\text{loss}} \sim d/2$, as we demonstrate in [Appendix E 2](#).
- **Ignoring nonlinear effects:** The Average-MLE decoder enumerates detector patterns from individual losses and combines them linearly. However, multiple simultaneous losses can produce detector patterns that cannot be decomposed into the sum of individual loss patterns. When such nonlinear patterns occur, the decoder must explain them using additional Pauli errors, degrading performance. This effect is particularly significant in the SWAP syndrome extraction as shown in [Appendix K](#).

VI. ENVELOPE-MATCHING DECODER

Matching-based decoders offer efficiency and natural compatibility with transversal logical circuits. Inspired by the exclusivity constraint of the Envelope-MLE decoder, we propose the Envelope-Matching decoder, which

achieves $d_{\text{loss}} \sim 2d/3$ for the Mid-SWAP syndrome extraction. This exceeds the $d_{\text{loss}} \sim d/2$ achieved by previous matching-based decoders and is higher than the effective distance for Pauli errors $d_{\text{pauli}} \sim d/2$. Consequently, asymptotically, atom-loss errors are negligible compared with Pauli errors.

Algorithm 2 (Envelope-Matching Decoder).

1. **Graph Initialization (assuming we decode the Z observable):** Construct a standard matching graph $G = (V, E)$ where vertices V correspond to X -detectors and edges E correspond to Pauli errors, connecting the detectors that each error flips. Initialize the weight of every edge $e \in E$ to $w_e = -\log \frac{p_e}{1-p_e}$ where p_e is the probability of this edge being triggered. Let w be the average weight of the edges in the matching graph.

2. **Loss Processing:** For each triggered atom loss readout r_m , find its Pauli envelope E_m . Then, for each edge $e = (u, v)$, where u and v can be triggered simultaneously by some Pauli errors in E_m , update the weight as follows:

Space-like edges (detectors u and v involving measurements on different ancilla qubits): $w_e \leftarrow 0.5w$.

Time-like edges (detectors u and v only involve measurements on the same ancilla qubit): $w_e \leftarrow 0.25w$.

3. **Matching:** Run the MWPM decoder on the matching graph G with the updated weights.

By reweighting the affected edges to weights comparable to regular edges, instead of reducing them to a constant weight (which is asymptotically negligible compared with Pauli error weights), the Envelope-Matching decoder approximately enforces the exclusivity constraint: selecting multiple edges within the same envelope is discouraged.

Lemma 6 (Failure Condition of Envelope-Matching decoder). *For the Envelope-Matching decoder, decoding failure in the presence of n_p Pauli errors and n_l atom losses requires*

$$2n_p + 1.5n_l \geq d. \quad (8)$$

Proof. The proof relies on the fact that after the reweighting, under the equal-edge-weight assumption $w_e = w$ used in Appendix D 1, the distance of the matching graph is reduced by at most $0.5w$ for each loss event, and each loss event can be matched with total weight at most $0.5w$. See Appendix D 1 for details. \square

With this lemma, we can show that the decoder achieves $d_{\text{loss}} \sim 2d/3$ for the Mid-SWAP syndrome extraction.

Theorem 4 (Failure Probability of Envelope-Matching decoder). *For the Mid-SWAP syndrome extraction with code distance d , subject to independent atom loss with rate p_{loss} and background Pauli errors with rate p_{pauli} , the failure probability of the Envelope-Matching decoder satisfies:*

$$P_{\text{fail}} = O\left(p_{\text{th}}^{-d}(p_{\text{loss}}^{d_{\text{loss}}} + p_{\text{pauli}}^{d_{\text{pauli}}})\right).$$

where $d_{\text{loss}} \sim 2d/3$ and $d_{\text{pauli}} \sim d/2$.

Proof. This follows from standard MWPM threshold analysis. See Appendix D 2 for details. \square

In contrast, the Marginal-Matching decoder [17, 18] computes the marginal probability that each atom is lost given the loss-resolving readout, adds depolarizing errors with strength proportional to these marginal probabilities, and runs a standard MWPM decoder. Like the Average-MLE decoder, it sets the edges that could be triggered to a constant weight, meaning no exclusivity constraint is enforced, limiting its effective distance to $d_{\text{loss}} \sim d/2$.

VII. EVALUATION

A. Experimental Setup

Error Model. We simulate a noise model combining circuit-level depolarizing noise (probability p_{pauli}) with atom loss (probability p_{loss}). First, we apply standard circuit-level Pauli errors: single-qubit gates, resets, measurements, and idling locations experience single-qubit depolarizing noise, while two-qubit gates ($CNOT$) experience two-qubit depolarizing noise, all with parameter p_{pauli} . Second, atom loss occurs after each operation. For two-qubit gates, loss occurs independently on each qubit with probability $p_{\text{loss}}/2$, so a two-qubit gate causes at least one loss with probability approximately p_{loss} , consistent with previous work [14]. Finally, loss-resolving readouts are also subject to errors: with probability $p_{\text{readout}}/2$, an existing atom is misidentified as lost, and with probability $p_{\text{readout}}/2$, a lost atom is misidentified as existing and assigned a random 0/1 outcome.

We parameterize the noise model using a total error rate p and a loss contribution $\eta \in [0, 1]$, where $p_{\text{readout}} = p_{\text{loss}} = p \cdot \eta$ and $p_{\text{pauli}} = p \cdot (1 - \eta)$.

Since most decoders calculate Pauli weights using $-\log \frac{p_{\text{pauli}}}{1-p_{\text{pauli}}}$, which is undefined when $p_{\text{pauli}} = 0$, we set $p_{\text{pauli}} = 10^{-9}$ for $\eta = 1$ to avoid numerical issues.

Software. We use Stim [32] for circuit simulation and sampling. For decoding, we employ PyMatching [33] for minimum-weight perfect matching implementations (Envelope-Matching decoder and Marginal-Matching decoder) and Gurobi v13 (with a 60-second timeout) for MILP-based decoders (Average-MLE decoder and Envelope-MLE decoder).

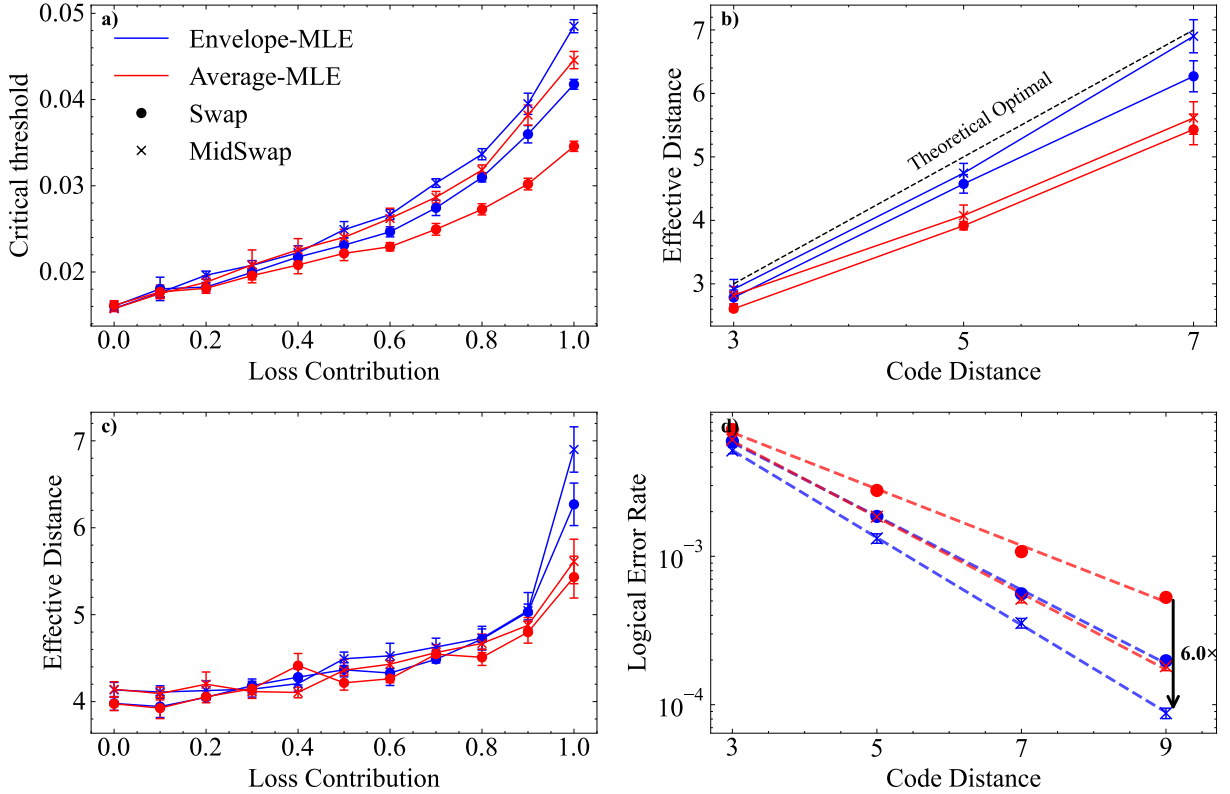


FIG. 9: Comparison of the Envelope-MLE decoder and the Average-MLE decoder on Mid-SWAP syndrome extraction and SWAP syndrome extraction: (a) threshold versus loss contribution η (ratio of atom loss to total error rate p); (b) effective distance versus code distance with $\eta = 1$; (c) effective distance at $d = 7$ versus loss contribution; and (d) distance scaling at $\eta = 90\%$ and total error rate $p = 1.5\%$.

Simulation parameters. We perform $3d$ rounds of syndrome extraction for code distance d to minimize boundary effects. For SWAP syndrome extraction and Mid-SWAP syndrome extraction, we alternate syndrome extraction rounds with different measurement orderings to ensure complete replenishment of all boundary data qubits. Hyperparameters for Envelope-Matching decoder are empirically optimized as described in Appendix J.

Data fitting. We extract effective distances using exponential fitting at low physical error rates $P_{\text{LER}} = \alpha(p_{\text{physical}}/p_{\text{th}})^{d_{\text{eff}}}$, and thresholds via critical-point fitting following [34] near the threshold regime $P_{\text{LER}} = a + bx + cx^2$ where $x = (p_{\text{physical}} - p_{\text{th}}) \times d^{1/\nu}$. MILP-based decoders are evaluated at $d \in \{5, 7\}$, while matching-based decoders are evaluated at $d \in \{5, 7, 9\}$ for threshold estimation.

B. Envelope-MLE Decoder vs Average-MLE Decoder

We compare the Envelope-MLE decoder against the Average-MLE decoder on the SWAP syndrome extraction and Mid-SWAP syndrome extraction. The teleportation circuit is excluded due to substantially inferior per-

formance (Appendix H).

Fig. 9 shows that Envelope-MLE decoder achieves higher thresholds and effective distances than Average-MLE decoder on both circuits, with Mid-SWAP syndrome extraction outperforming SWAP syndrome extraction in all cases. Combining Envelope-MLE decoder with Mid-SWAP syndrome extraction improves the threshold from 3.46% to 4.85%, a 40% increase over prior work. Specifically, at loss contribution $\eta = 1$, Envelope-MLE decoder achieves $d_{\text{loss}} \approx 7$ for distance-7 Mid-SWAP syndrome extraction, matching the theoretical optimum. When the total error rate is $p = 1.5\%$ and loss contribution is $\eta = 90\%$, we achieve $6\times$ error suppression over previous work.

C. Envelope-MLE Decoder on Experimental Data

We evaluate the Envelope-MLE decoder on recent experimental data reported by Ref. [10]. As shown in Fig. 10, replacing the Average-MLE decoder with the Envelope-MLE decoder improves the error suppression factor from $\Lambda = 1.69 \pm 0.08$ to $\Lambda = 2.01 \pm 0.11$. When combined with a machine-learning decoder, the Envelope-MLE decoder further increases Λ from $2.14 \pm$

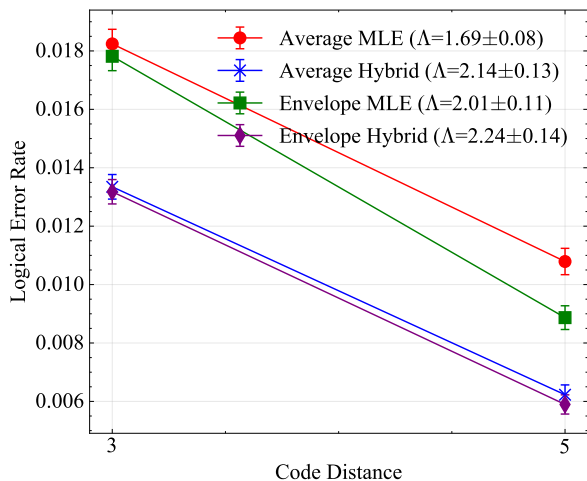


FIG. 10: Per-round logical error rate and error suppression factor Λ ($P_{\text{LER}}^{d=3}/P_{\text{LER}}^{d=5}$) evaluated on experimental data from Ref. [10]. Hybrid refers to combining an MLE decoder with a machine-learning decoder. Replacing the Average-MLE decoder with the Envelope-MLE decoder improves Λ both as a standalone decoder (from 1.69 to 2.01) and when combined with a machine-learning decoder (from 2.14 to 2.24).

0.13 to 2.24 ± 0.14 , demonstrating that our framework provides complementary gains on top of learned decoders.

D. Envelope-Matching Decoder vs Marginal-Matching Decoder

We evaluate our scalable Envelope-Matching decoder against the Marginal-Matching decoder on SWAP syndrome extraction and Mid-SWAP syndrome extraction. The Marginal-Matching decoder was originally designed for erasure errors with delayed checks and is therefore not fully aware of the error model of atom loss; nevertheless, we adopt it as our baseline since it represents the best available matching-based decoder from prior work. Concretely, we supply Marginal-Matching decoder with an error model in which each atom loss is replaced by an erasure error with full depolarization, as this is the closest approximation to atom loss within its supported error model. Fig. 11 shows that Envelope-Matching decoder achieves substantially higher thresholds and effective distances on both circuits, with Mid-SWAP syndrome extraction consistently outperforming SWAP syndrome extraction. Combining Envelope-Matching decoder with Mid-SWAP syndrome extraction improves the threshold from 3.42% to 4.38%, a 30% increase over prior work.

Marginal-Matching decoder exhibits severe performance degradation as $\eta \rightarrow 1$: as $p_{\text{pauli}} \rightarrow 0$, the Pauli weights $-\log \frac{p_{\text{pauli}}}{1-p_{\text{pauli}}} \rightarrow \infty$, while loss-induced edges retain constant weight, causing the decoder to over-select loss-induced edges. Theoretical analysis confirms that

Marginal-Matching decoder is limited to $d_{\text{loss}} \sim d/2$ (Appendix E 1), whereas our approach achieves $d_{\text{loss}} \sim 2d/3$.

E. Compatibility with Transversal Logical Circuits

Beyond memory experiments, we evaluate Envelope-Matching decoder on transversal logical circuits. We consider a two-logical-qubit circuit that repeatedly performs transversal *CNOT* gates (with the first qubit as control and the second as target) after each syndrome extraction cycle, followed by a logical *Z* measurement on the target qubit. Fig. 12 shows that Envelope-Matching decoder with Mid-SWAP syndrome extraction achieves higher thresholds and effective distances than Marginal-Matching decoder, demonstrating that our approach naturally extends to logical circuit decoding.

VIII. SUMMARY AND OUTLOOK

We have presented the Pauli envelope, a theoretical framework for analyzing atom loss in neutral-atom quantum computers. Using this framework, we designed the Mid-SWAP syndrome extraction, a syndrome extraction circuit that achieves an optimal effective distance for atom loss $d_{\text{loss}} \sim d$ with the Envelope-MLE decoder, and $d_{\text{loss}} \sim 2d/3$ with the efficient Envelope-Matching decoder.

Our results demonstrate that atom loss, despite requiring destructive detection, can achieve the same effective distance as erasure errors and a much higher threshold than Pauli errors. This establishes that atom loss errors will not be a bottleneck for the scalability of neutral-atom quantum computers and provides new insights for future hardware and decoder co-design.

Several directions remain open for future work. First, we briefly discuss how to extend our techniques to general CSS codes and correlated atom loss in Appendices F and G. Interestingly, we find that the threshold increases gradually from 5% to 8% as the correlated atom loss contribution increases. This suggests that, in this setting, correlated atom-loss events can be easier to tolerate than independent atom loss and should not be a bottleneck in fault-tolerant quantum computing. However, more detailed analysis is needed. Second, the performance gap between Envelope-MLE decoder and Envelope-Matching decoder suggests room for intermediate decoders that balance optimality and efficiency. Third, dual-rail superconducting qubits exhibit a similar error model as atom loss. Applying our framework to this platform is a promising direction. Finally, the Pauli envelope can serve as an input feature for machine learning-based decoders like those in [35], potentially improving their interpretability and generalization.

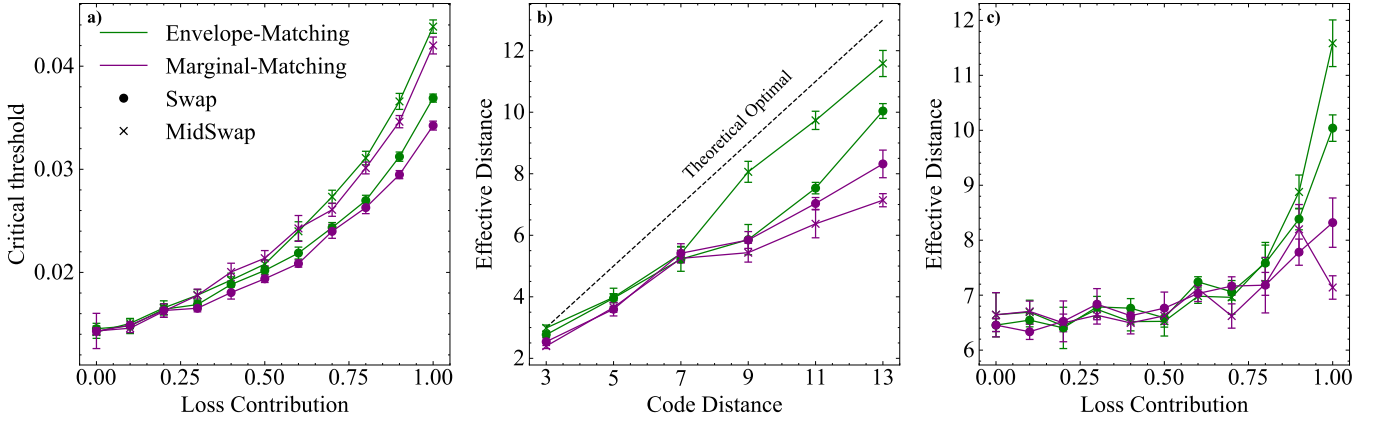


FIG. 11: Comparison of the Envelope-Matching decoder and the Marginal-Matching decoder on Mid-SWAP syndrome extraction and SWAP syndrome extraction: (a) threshold versus loss contribution; (b) effective distance versus code distance with $\eta = 1$; (c) effective distance at $d = 13$ versus loss contribution.

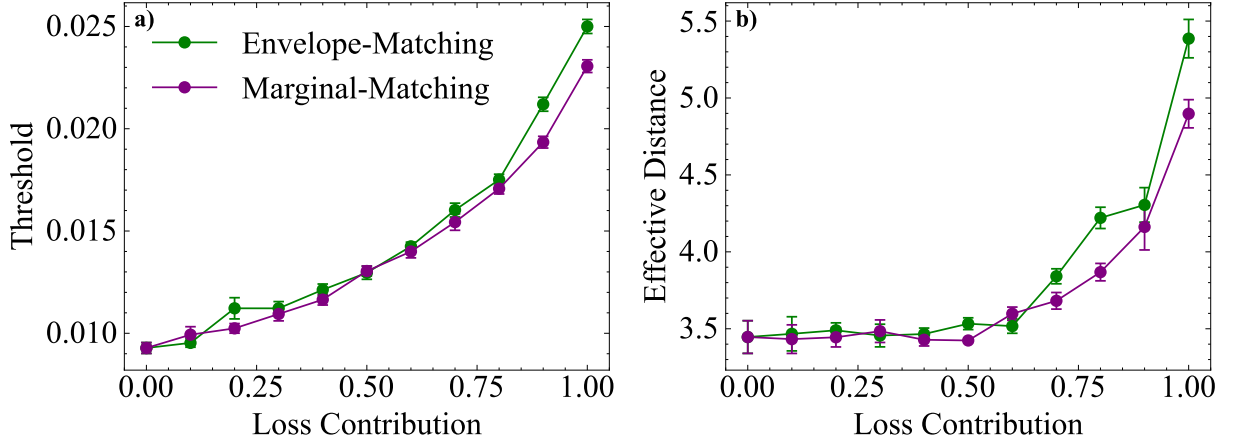


FIG. 12: Comparison of the Envelope-Matching decoder and the Marginal-Matching decoder for transversal logical circuits with Mid-SWAP syndrome extraction: (a) threshold versus loss contribution; (b) effective distance at $d = 7$ versus loss contribution.

ACKNOWLEDGMENTS

We thank G. Baranes, J. P. Bonilla Ataides, H. Dehghani, C. Duckering, S. Gu, A. Kubica, M. D. Lukin, and Y. Wu for helpful discussions and comments on the manuscript. P.L. and U.A. are supported by NSF grants CCF-1901381, CCF-2115104, CCF-2119352, and CCF-2107241. We are grateful to Chameleon Cloud for pro-

viding the computing cycles needed for the experiments. S.J.S.T. acknowledges support from the National University of Singapore (NUS) Development Grant. E.H. is supported by the Fulbright Future Scholarship. H.Z. and C.Z. are supported by IARPA and the Army Research Office under the Entangled Logical Qubits program (Cooperative Agreement Number W911NF-23-2-0219) and the DARPA MeasQuIT program (HR0011-24-9-0359).

-
- [1] P. W. Shor, Algorithms for quantum computation: discrete logarithms and factoring, in *Proceedings 35th annual symposium on foundations of computer science* (Ieee, 1994) pp. 124–134.
- [2] A. J. Daley, I. Bloch, C. Kokail, S. Flannigan, N. Pearson, M. Troyer, and P. Zoller, Practical quantum advantage in quantum simulation, *Nature* **607**, 667 (2022).
- [3] M. Cerezo, A. Arrasmith, R. Babbush, S. C. Benjamin, S. Endo, K. Fujii, J. R. McClean, K. Mitarai, X. Yuan, L. Cincio, *et al.*, Variational quantum algorithms, *Nature Reviews Physics* **3**, 625 (2021).
- [4] D. Gottesman, Surviving as a quantum computer in a classical world, *Textbook manuscript preprint* **8**, 8 (2024).

- [5] E. Dennis, A. Kitaev, A. Landahl, and J. Preskill, Topological quantum memory, *Journal of Mathematical Physics* **43**, 4452 (2002).
- [6] A. G. Fowler, M. Mariantoni, J. M. Martinis, and A. N. Cleland, Surface codes: Towards practical large-scale quantum computation, *Physical Review A—Atomic, Molecular, and Optical Physics* **86**, 032324 (2012).
- [7] S. J. S. Tan, C. A. Pattison, M. McEwen, and J. Preskill, Resilience of the surface code to error bursts, arXiv preprint arXiv:2406.18897 (2024).
- [8] J. D. Chadwick, C. Kang, J. Vizslai, S. F. Lin, and F. T. Chong, Averting multi-qubit burst errors in surface code magic state factories, in *2024 IEEE International Conference on Quantum Computing and Engineering (QCE)*, Vol. 1 (IEEE, 2024) pp. 1089–1101.
- [9] N.-C. Chiu, E. C. Trapp, J. Guo, M. H. Aboeih, L. M. Stewart, S. Hollerith, P. L. Stroganov, M. Kalinowski, A. A. Geim, S. J. Evered, *et al.*, Continuous operation of a coherent 3,000-qubit system, *Nature*, 1 (2025).
- [10] D. Bluvstein, A. A. Geim, S. H. Li, S. J. Evered, J. P. Bonilla Ataides, G. Baranes, A. Gu, T. Manovitz, M. Xu, M. Kalinowski, *et al.*, A fault-tolerant neutral-atom architecture for universal quantum computation, *Nature*, 1 (2025).
- [11] B. W. Reichardt, A. Paetznick, D. Aasen, I. Basov, J. M. Bello-Rivas, P. Bonderson, R. Chao, W. van Dam, M. B. Hastings, A. Paz, *et al.*, Logical computation demonstrated with a neutral atom quantum processor, arXiv e-prints, arXiv (2024).
- [12] M. Schlosser, S. Tichelmann, D. Schäffner, D. O. de Mello, M. Hambach, J. Schütz, and G. Birkl, Scalable multilayer architecture of assembled single-atom qubit arrays in a three-dimensional talbot tweezer lattice, *Phys. Rev. Lett.* **130**, 180601 (2023).
- [13] L. Pause, L. Sturm, M. Mittenbühler, S. Amann, T. Preuschoff, D. Schäffner, M. Schlosser, and G. Birkl, Supercharged two-dimensional tweezer array with more than 1000 atomic qubits, *Optica* **11**, 222 (2024).
- [14] G. Baranes, M. Cain, J. P. B. Ataides, D. Bluvstein, J. Sinclair, V. Vuletić, H. Zhou, and M. D. Lukin, Leveraging qubit loss detection in fault-tolerant quantum algorithms, *Physical Review X* **16**, 011002 (2026).
- [15] C.-C. Yu, Y.-H. Deng, M.-C. Chen, C.-Y. Lu, and J.-W. Pan, Locating rydberg decay error in swap-lru, arXiv preprint arXiv:2503.01649 (2025).
- [16] C.-C. Yu, Z.-H. Chen, Y.-H. Deng, M.-C. Chen, C.-Y. Lu, and J.-W. Pan, Processing and decoding rydberg decay error with mbqc, arXiv preprint arXiv:2411.04664 (2024).
- [17] S. Gu, A. Retzker, and A. Kubica, Fault-tolerant quantum architectures based on erasure qubits, *Physical Review Research* **7**, 013249 (2025).
- [18] S. Gu, Y. Vaknin, A. Retzker, and A. Kubica, Optimizing quantum error correction protocols with erasure qubits, arXiv preprint arXiv:2408.00829 (2024).
- [19] M. Cain, D. Bluvstein, C. Zhao, S. Gu, N. Maskara, M. Kalinowski, A. A. Geim, A. Kubica, M. D. Lukin, and H. Zhou, Fast correlated decoding of transversal logical algorithms, arXiv preprint arXiv:2505.13587 (2025).
- [20] H. Zhou, C. Zhao, M. Cain, D. Bluvstein, C. Duckering, H.-Y. Hu, S.-T. Wang, A. Kubica, and M. D. Lukin, Algorithmic fault tolerance for fast quantum computing, arXiv preprint arXiv:2406.18897 (2024).
- [21] M. Serra-Peralta, M. H. Shaw, and B. M. Terhal, Decoding across transversal clifford gates in the surface code, arXiv preprint arXiv:2505.13599 (2025).
- [22] H. Levine, A. Haim, J. S. Hung, N. Alidoust, M. Kalae, L. DeLorenzo, E. A. Wollack, P. Arrangoiz-Arriola, A. Khalajhedayati, R. Sanil, *et al.*, Demonstrating a long-coherence dual-rail erasure qubit using tunable transmons, *Physical Review X* **14**, 011051 (2024).
- [23] N. Mehta, J. D. Teoh, T. Noh, A. Agrawal, A. Anderson, B. Birdsall, A. Brahmabhatt, W. Byrd, M. Cacioppo, A. Cabrera, *et al.*, Bias-preserving and error-detectable entangling operations in a superconducting dual-rail system, arXiv preprint arXiv:2503.10935 (2025).
- [24] K. S. Chou, T. Shemma, H. McCarrick, T.-C. Chien, J. D. Teoh, P. Winkel, A. Anderson, J. Chen, J. C. Curtis, S. J. de Graaf, *et al.*, A superconducting dual-rail cavity qubit with erasure-detected logical measurements, *Nature Physics* **20**, 1454 (2024).
- [25] Y. Wu, S. Kolkowitz, S. Puri, and J. D. Thompson, Erasure conversion for fault-tolerant quantum computing in alkaline earth rydberg atom arrays, *Nature communications* **13**, 4657 (2022).
- [26] The circuit output may be nondeterministic even with fixed errors; we implicitly fix the randomness for simplicity. Also, when the context is clear, we drop the subscript C .
- [27] J. Ghosh, A. G. Fowler, J. M. Martinis, and M. R. Geller, Understanding the effects of leakage in superconducting quantum-error-detection circuits, *Physical Review A* **88**, 062329 (2013).
- [28] M. Suchara, A. W. Cross, and J. M. Gambetta, Leakage suppression in the toric code, in *2015 IEEE International Symposium on Information Theory (ISIT)* (IEEE, 2015) pp. 1119–1123.
- [29] M. N. Chow, V. Buchemavari, S. Omanakuttan, B. J. Little, S. Pandey, I. H. Deutsch, and Y.-Y. Jau, Circuit-based leakage-to-erasure conversion in a neutral-atom quantum processor, *PRX Quantum* **5**, 040343 (2024).
- [30] H. Perrin, S. Jandura, and G. Pupillo, Quantum error correction resilient against atom loss, arXiv preprint arXiv:2412.07841 (2024).
- [31] There will be interaction terms like $p_{\text{loss}}p_{\text{pauli}}$ in the exact expression, but they are bounded by $p_{\text{loss}}^2 + p_{\text{pauli}}^2$ so will not appear in the scaling.
- [32] C. Gidney, Stim: a fast stabilizer circuit simulator, *Quantum* **5**, 497 (2021).
- [33] O. Higgott, Pymatching: A python package for decoding quantum codes with minimum-weight perfect matching, *ACM Transactions on Quantum Computing* **3**, 1 (2022).
- [34] C. Wang, J. Harrington, and J. Preskill, Confinement-higgs transition in a disordered gauge theory and the accuracy threshold for quantum memory, *Annals of Physics* **303**, 31 (2003).
- [35] J. P. Bonilla Ataides, A. Gu, S. F. Yelin, and M. D. Lukin, Neural decoders for universal quantum algorithms, arXiv e-prints, arXiv (2025).
- [36] A. A. Kovalev and L. P. Pryadko, Fault tolerance of quantum low-density parity check codes with sublinear distance scaling, *Physical Review A—Atomic, Molecular, and Optical Physics* **87**, 020304 (2013).
- [37] J.-P. Tillich and G. Zemor, Quantum LDPC codes with positive rate and minimum distance proportional to the square root of the blocklength, *IEEE Transactions on Information Theory* **60**, 1193 (2014).

- [38] S. Bravyi, A. W. Cross, J. M. Gambetta, D. Maslov, P. Rall, and T. J. Yoder, High-threshold and low-overhead fault-tolerant quantum memory, *Nature* **627**, 778 (2024).
- [39] A. G. Manes and J. Claes, Distance-preserving stabilizer measurements in hypergraph product codes, *Quantum* **9**, 1618 (2025).
- [40] S. J. S. Tan and L. Stambler, Effective distance of higher dimensional hqps and weight-reduced quantum ldpc codes, *Quantum* **9**, 1897 (2025).
- [41] E. T. Campbell, A theory of single-shot error correction for adversarial noise, *Quantum Science and Technology* **4**, 025006 (2019).
- [42] A. O. Quintavalle, M. Vasmer, J. Roffe, and E. T. Campbell, Single-shot error correction of three-dimensional homological product codes, *PRX Quantum* **2**, 020340 (2021).
- [43] N. Berthussen, S. J. S. Tan, E. Huang, and D. Gottesman, Adaptive syndrome extraction, *PRX Quantum* **6**, 030307 (2025).
- [44] Y. Hong, Single-shot preparation of hypergraph product codes via dimension jump, *Quantum* **9**, 1879 (2025).
- [45] A. O. Quintavalle, P. Webster, and M. Vasmer, Partitioning qubits in hypergraph product codes to implement logical gates, *Quantum* **7**, 1153 (2023).
- [46] G. Zhu, S. Sikander, E. Portnoy, A. W. Cross, and B. J. Brown, Non-clifford and parallelizable fault-tolerant logical gates on constant and almost-constant rate homological quantum ldpc codes via higher symmetries, arXiv preprint arXiv:2310.16982 (2023).
- [47] N. P. Breuckmann and S. Burton, Fold-transversal clifford gates for quantum codes, *Quantum* **8**, 1372 (2024).
- [48] N. P. Breuckmann, M. Davydova, J. N. Eberhardt, and N. Tantivasadakarn, Cups and gates i: Cohomology invariants and logical quantum operations, arXiv preprint arXiv:2410.16250 (2024).
- [49] T.-C. Lin, Transversal non-clifford gates for quantum ldpc codes on sheaves, arXiv preprint arXiv:2410.14631 (2024).
- [50] Q. Xu, H. Zhou, G. Zheng, D. Bluvstein, J. P. B. Ataiades, M. D. Lukin, and L. Jiang, Fast and parallelizable logical computation with homological product codes, *Physical Review X* **15**, 021065 (2025).
- [51] N. Berthussen, M. J. Gullans, Y. Hong, M. Mudassar, and S. J. S. Tan, Automorphism gadgets in homological product codes, arXiv preprint arXiv:2508.04794 (2025).
- [52] L. Golowich, K. Chang, and G. Zhu, Constant-overhead addressable gates via single-shot code switching, arXiv preprint arXiv:2510.06760 (2025).
- [53] L. Golowich and T.-C. Lin, Quantum ldpc codes with transversal non-clifford gates via products of algebraic codes, in *Proceedings of the 57th Annual ACM Symposium on Theory of Computing* (2025) pp. 689–696.
- [54] G. Zhu, A topological theory for qldpc: non-clifford gates and magic state fountain on homological product codes with constant rate and beyond the $N^{1/3}$ distance barrier, arXiv preprint arXiv:2501.19375 (2025).
- [55] G. Zhu, Transversal non-clifford gates on qldpc codes breaking the \sqrt{N} distance barrier and quantum-inspired geometry with \mathbb{Z}_2 systolic freedom, arXiv preprint arXiv:2507.15056 (2025).
- [56] S. J. S. Tan, Y. Hong, T.-C. Lin, M. J. Gullans, and M.-H. Hsieh, Single-shot universality in quantum ldpc codes via code-switching, arXiv preprint arXiv:2510.08552 (2025).
- [57] C. Li, J. Preskill, and Q. Xu, Transversal dimension jump for product qldpc codes, arXiv preprint arXiv:2510.07269 (2025).
- [58] C. Gidney, [Preserving distance during stabilizer measurements by alternating interaction order from round to round](#), Quantum Computing Stack Exchange (2025), accessed: 2025.
- [59] Y. Lin, A. Anand, and K. R. Brown, Dynamic local single-shot checks for toric codes, arXiv preprint arXiv:2511.20576 (2025).

Appendix A: Proofs from Pauli Envelope Section

This section contains the detailed proofs of lemmas and theorems presented in the Pauli envelope section.

1. Proof of Effective Distance Theorem

Theorem 1 (Logical Error Rate is Upper-Bounded by Failure Probability).

$$P_{\text{LER}}(\mathcal{C}, \mathcal{P}_l, \mathcal{P}_p, \text{Dec}) \leq P_{\text{fail}}(\mathcal{C}, \mathcal{P}_l, \mathcal{P}_p, \text{Dec}).$$

Proof. Consider any loss configuration l with readout $r = \mathcal{R}(l)$ and Pauli error p . Let E denote the Pauli envelope of r . By Lemma 1, if $\text{Dec}(\cdot, r)$ correctly decodes all detector-observable pairs in $\mathcal{S}(p \oplus E, \emptyset)$, then it also correctly decodes all pairs in $\mathcal{S}(p, \mathcal{L}(r))$.

Taking the contrapositive: for any realization (p, l) where the decoder fails, i.e., $\text{Dec}(\mathcal{D}(p, l), \mathcal{R}(l)) \neq \mathcal{O}(p, l)$, there must exist some $(\mathcal{D}, \mathcal{O}) \in \mathcal{S}(p \oplus E, \emptyset)$ such that $\text{Dec}(\mathcal{D}, \mathcal{R}(l)) \neq \mathcal{O}$.

Taking expectation over all loss configurations and Pauli errors, we obtain

$$\begin{aligned} & P_{\text{LER}}(\mathcal{C}, \mathcal{P}_l, \mathcal{P}_p, \text{Dec}) \\ &= \Pr_{\substack{l \sim \mathcal{P}_l \\ p \sim \mathcal{P}_p}} [\text{Dec}(\mathcal{D}(p, l), \mathcal{R}(l)) \neq \mathcal{O}(p, l)] \\ &\leq \Pr_{\substack{l \sim \mathcal{P}_l \\ p \sim \mathcal{P}_p}} [\exists (\mathcal{D}, \mathcal{O}) \in \mathcal{S}(p \oplus E, \emptyset) : \text{Dec}(\mathcal{D}, \mathcal{R}(l)) \neq \mathcal{O}] \\ &= P_{\text{fail}}(\mathcal{C}, \mathcal{P}_l, \mathcal{P}_p, \text{Dec}). \end{aligned}$$

□

2. Proof of Pauli Envelope of Atom Loss

Lemma 2 (Pauli Envelope of Atom Loss). *Let \mathcal{C} be a Clifford circuit and l be an atom loss configuration corresponding to a single atom loss location. Then the following construction yields a Pauli envelope E for l .*

Let $L_i = \{I, X, Y, Z\}$ denote the set of all single-qubit Pauli operators at a specific space-time location i . For two such sets, we define $L_i \oplus L_j = \{e_i \oplus e_j : e_i \in L_i, e_j \in L_j\}$ as the set of all pairwise compositions. We identify the relevant locations: (1) the loss location itself, (2) immediately after each subsequent Hadamard gate acting on the lost atom, and (3) just before measuring the lost atom. The Pauli envelope is then $E = L_1 \oplus L_2 \oplus \dots \oplus L_k$, where L_1, \dots, L_k are the Pauli sets at these relevant locations.

Proof. We construct a sequence of equivalent circuits, illustrated in Fig. 13.

Step 1 ($\mathcal{C} \rightarrow \mathcal{C}_1$): Insert a reset gate after every gate following the loss event. Since the lost atom is in the $|0\rangle$ state, all the CZ gates have no effect.

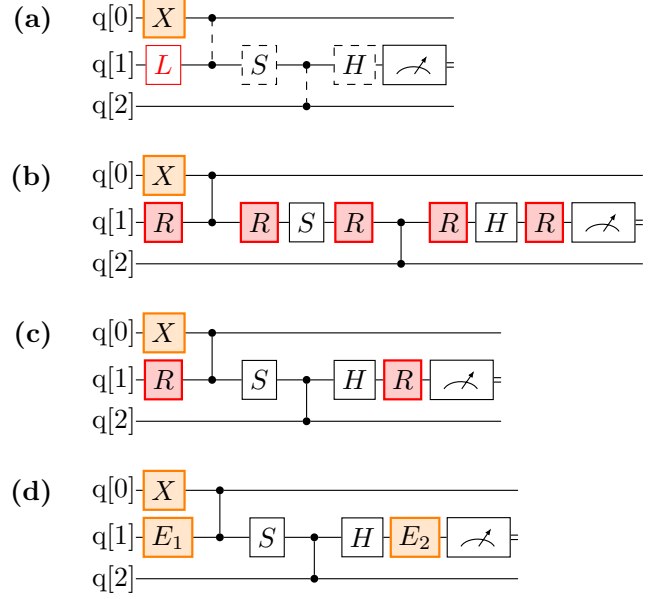


FIG. 13: Construction of the Pauli envelope for atom loss. The orange X gate represents a Pauli error p . (a) Original circuit \mathcal{C} with a loss event L on qubit q_1 . (b) Circuit \mathcal{C}_1 where reset gates are inserted after every gate following the loss. (c) Circuit \mathcal{C}_2 where resets are only at key locations: the loss location, after each Hadamard gate, and before measurement. CZ and S gates preserve $|0\rangle$, so intermediate resets are redundant. (d) Circuit \mathcal{C}_3 , which is equivalent to \mathcal{C} with Pauli envelope $E_1 \oplus E_2$, where $E_1 = E_2 = \{I, X, Y, Z\}$.

We use $\mathcal{S}(\mathcal{C})$ to denote the set of possible outcomes of \mathcal{C} . By our modeling of atom loss, $\mathcal{S}(\mathcal{C}) = \mathcal{S}(\mathcal{C}_1)$.

Step 2 ($\mathcal{C}_1 \rightarrow \mathcal{C}_2$): Retain resets only at three key locations: (1) the loss location, (2) immediately after each subsequent Hadamard gate on the lost atom, and (3) just before measurement. Since CZ and S gates preserve the $|0\rangle$ state, the intermediate resets are redundant, giving $\mathcal{S}(\mathcal{C}_1) = \mathcal{S}(\mathcal{C}_2)$.

Step 3 ($\mathcal{C}_2 \rightarrow$ Pauli envelope): Let E denote all possible Pauli errors at these three types of locations. Since each reset can be expressed as a probabilistic mixture of Pauli operators, we have $\mathcal{S}(\mathcal{C}_2) \subseteq \mathcal{S}(\mathcal{C}_3)$.

Notice \mathcal{C}_3 is just \mathcal{C} with Pauli envelope E , and none of the above derivations depends on whether there are additional Pauli errors. Combining these steps, we have $\forall p, \mathcal{S}(p, l) \subseteq \mathcal{S}(p \oplus E, \emptyset)$. □

3. Proof of Pauli Envelope for Multiple Losses

Lemma 3 (Linearity of Pauli Envelope). (a) Consider a loss configuration $l = l_1 \oplus l_2 \oplus \dots \oplus l_k$, where each l_i is a single-atom loss configuration. The following composition yields a Pauli envelope for l : $E(l) = \bigoplus_{i=1}^k E(l_i)$.

(b) For a readout r corresponding to a single atom

loss with multiple possible loss configurations $\mathcal{L}(r) = \{l^{(1)}, l^{(2)}, \dots\}$, the following union yields a Pauli envelope for r : $E(r) = \bigcup_{l \in \mathcal{L}(r)} E(l)$.

(c) For a readout $r = r_1 \oplus r_2 \oplus \dots \oplus r_m$, where each r_i is a single-atom loss readout corresponding to m atom losses, the following composition yields a Pauli envelope for r : $E(r) = \bigoplus_{i=1}^m E(r_i)$.

Proof. Part (a): Consider a loss configuration $l = l_1 \oplus l_2 \oplus \dots \oplus l_k$ with k loss locations. We construct a sequence of circuits $\mathcal{C}_0, \mathcal{C}_1, \dots, \mathcal{C}_k$, where \mathcal{C}_i is obtained from \mathcal{C}_{i-1} by removing the gates affected by loss l_i , thus $\mathcal{S}_{\mathcal{C}_i}(p, \emptyset) = \mathcal{S}_{\mathcal{C}_{i-1}}(p, l_i)$. Let $E(l_i)$ denote the Pauli envelope for loss l_i . Applying Lemma 2 to the transition from \mathcal{C}_{i-1} to \mathcal{C}_i , we have $\mathcal{S}_{\mathcal{C}_i}(p, \emptyset) = \mathcal{S}_{\mathcal{C}_{i-1}}(p, l_i) \subseteq \mathcal{S}_{\mathcal{C}_{i-1}}(p \oplus E(l_i), \emptyset)$. Iterating this relation backwards from k to 0, we obtain

$$\begin{aligned} \mathcal{S}_{\mathcal{C}}(p, l) &= \mathcal{S}_{\mathcal{C}_k}(p, \emptyset) \\ &\subseteq \mathcal{S}_{\mathcal{C}_{k-1}}(p \oplus E(l_k), \emptyset) \\ &\subseteq \mathcal{S}_{\mathcal{C}_{k-2}}(p \oplus E(l_k) \oplus E(l_{k-1}), \emptyset) \\ &\vdots \\ &\subseteq \mathcal{S}_{\mathcal{C}_0} \left(p \oplus \bigoplus_{i=1}^k E(l_i), \emptyset \right). \end{aligned}$$

Thus $E(l) = \bigoplus_{i=1}^k E(l_i)$ is a valid Pauli envelope.

Part (b): For a readout r with possible loss configurations $\mathcal{L}(r) = \{l^{(1)}, l^{(2)}, \dots\}$, we have $\mathcal{S}(p, \mathcal{L}(r)) = \bigcup_{l \in \mathcal{L}(r)} \mathcal{S}(p, l)$. By definition, $\mathcal{S}(p, l) \subseteq \mathcal{S}(p \oplus E(l), \emptyset)$, so $\mathcal{S}(p, \mathcal{L}(r)) \subseteq \bigcup_l \mathcal{S}(p \oplus E(l), \emptyset) = \mathcal{S}(p \oplus \bigcup_l E(l), \emptyset)$. Thus $E(r) = \bigcup_{l \in \mathcal{L}(r)} E(l)$.

Part (c): For $r = r_1 \oplus \dots \oplus r_m$, the possible configurations are $\mathcal{L}(r) = \{l_1 \oplus \dots \oplus l_m : l_i \in \mathcal{L}(r_i)\}$. By part (a), $E(l_1 \oplus \dots \oplus l_m) = \bigoplus_i E(l_i)$. By part (b), $E(r) = \bigcup_{(l_1, \dots, l_m)} \bigoplus_i E(l_i) = \bigoplus_i \bigcup_{l_i} E(l_i) = \bigoplus_i E(r_i)$, where the second equality uses the distributive property $(A \cup B) \oplus (C \cup D) = (A \oplus C) \cup (A \oplus D) \cup (B \oplus C) \cup (B \oplus D)$. \square

Appendix B: Detector Patterns from a Single Atom Loss

In this section, we illustrate how each atom loss event triggers a set of detector flips. For simplicity, we assume that the final observable is Z and only consider Z -type errors as these are already sufficient for our proofs. The detector patterns for both Mid-SWAP syndrome extraction and SWAP syndrome extraction are shown in Fig. 14.

1. Mid-SWAP Syndrome Extraction

The detector patterns for Mid-SWAP syndrome extraction are shown in Fig. 14a and Fig. 14c when a loss-resolving readout is triggered on X - and Z -type ancilla qubits, respectively. To generate these figures, we first

convert each atom loss event to its Pauli envelope, then identify all affected edges in the matching graph. These results will be sufficient for the proof of Lemma 4.

2. SWAP Syndrome Extraction

For SWAP syndrome extraction, the detector patterns are shown in Fig. 14b and Fig. 14d when a loss-resolving readout is triggered on X - and Z -type ancilla qubits, respectively. In this case, we do not convert the atom loss event to its Pauli envelope, but instead directly identify all affected edges by removing the gates that act on the lost atom. This approach is used because these figures will be employed to prove the upper bound on the effective distance in the next section, where we need to ensure that the failure events can actually occur due to atom loss.

Appendix C: Proofs from Envelope-MLE decoder Section

This section contains the detailed proofs of lemmas and theorems from the Envelope-MLE decoder section.

1. Proof of Optimality of Envelope-MLE decoder

Lemma 5 (Optimality of Envelope-MLE decoder). *The Envelope-MLE decoder finds a solution with Pauli weight no greater than that of the actual error configuration.*

Proof. According to Lemma 2, the Pauli envelope E constructed for each loss configuration satisfies the property that any detector-observable pair produced by the circuit with loss can also be produced by the circuit with errors from E and no loss.

Therefore, the actual error configuration (consisting of actual Pauli errors and loss events with their corresponding Pauli envelopes) is a feasible solution to the MILP.

Since the MILP minimizes the total Pauli error weight over all feasible solutions, and the actual error is feasible, the optimal solution found by the decoder must have weight no greater than the weight of the actual error. \square

2. Proof of Loss Pattern Weight Requirement

To analyze the decoder's failure conditions, we consider the difference between the actual error and the decoder's solution. Let C be the symmetric difference (XOR sum) of the actual error configuration and the decoder's output. Since both configurations satisfy the same detector syndrome constraints, C must have an empty syndrome. We define an *undetected logical error* as a configuration that produces an empty syndrome but implements a non-trivial logical operation (i.e., it is not a product of

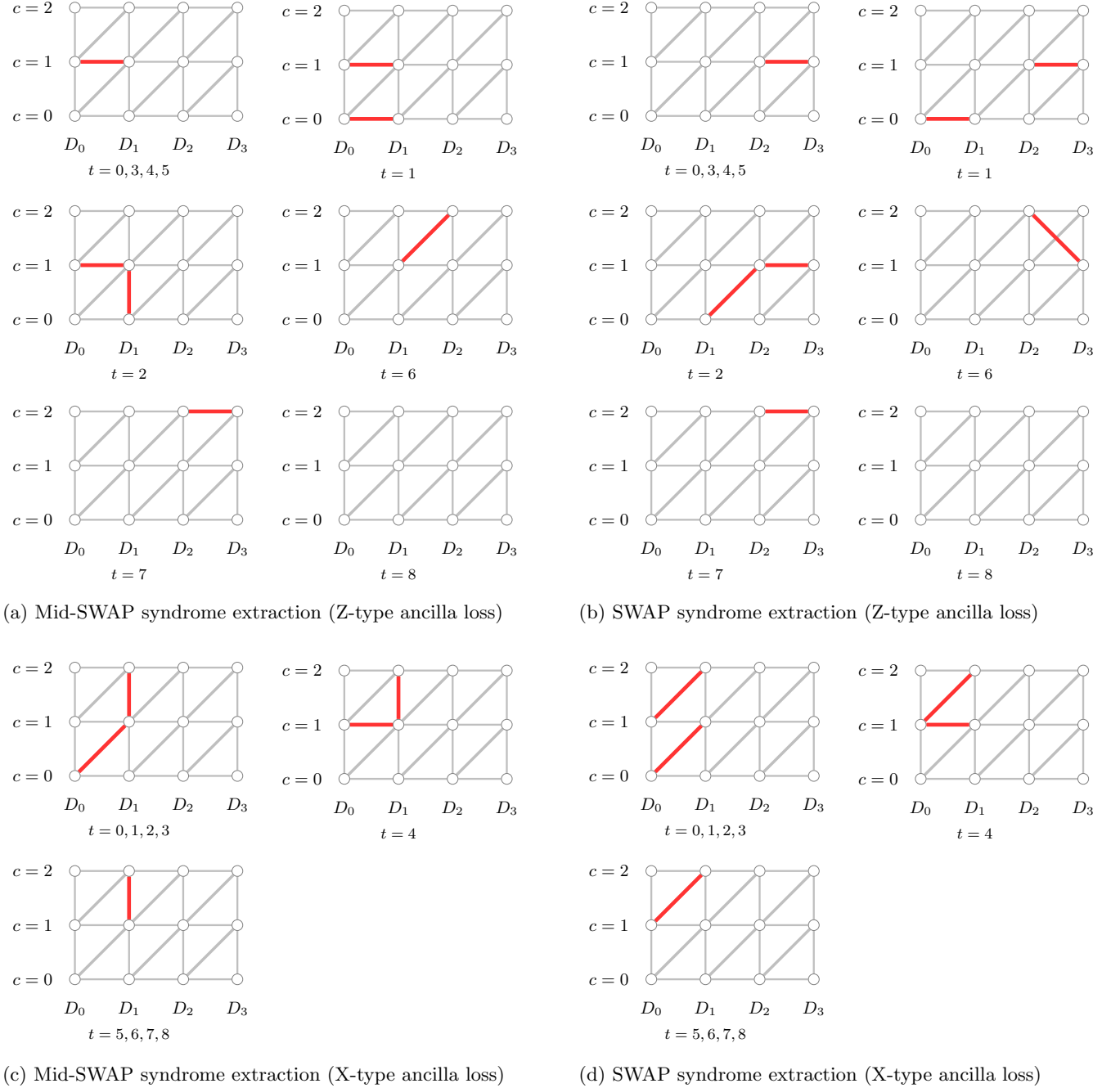


FIG. 14: Loss-induced detector patterns for different surface code variants. Each red edge can be triggered independently and will flip its two endpoints. This is a flattened view of the S_1 - S_2 - S_3 path as shown in Fig. 8. t represents the time step (the number of $CNOT$ gates since the last reset) when the atom loss event occurs. c represents the index of syndrome extraction rounds.

stabilizer generators). If the decoder fails, C represents such an error.

We decompose C into a Pauli component C_P (the XOR sum of Pauli errors) and a loss component consisting of mismatches in the selected loss patterns. Specifically, if for n_l loss events the decoder selects a different pattern \mathcal{D}_{m_i, k_i} than the actual one \mathcal{D}_{m_i, j_i} , these mismatches gen-

erate a syndrome difference $\bigoplus_{i=1}^{n_l} (\mathcal{D}_{m_i, j_i} \oplus \mathcal{D}_{m_i, k_i})$ that must be compensated by C_P to ensure the total syndrome is empty. With this setup, we can prove the following lemma.

Lemma 7. *For the Mid-SWAP syndrome extraction with distance d , if the combined error corresponding to C_P and syndrome difference $\bigoplus_{i=1}^{n_l} (\mathcal{D}_{m_i, j_i} \oplus \mathcal{D}_{m_i, k_i})$ forms an*

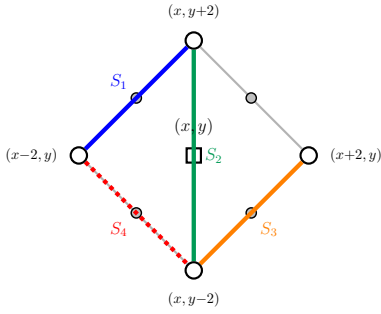


FIG. 15: Detector patterns from a single atom loss in the Mid-SWAP syndrome extraction. This is a zoomed-in view of the diamond structure in Fig. 8.

undetectable logical error, then $|C_P| \geq d - n_l$ where n_l is the number of loss events, and $|\cdot|$ denotes the number of errors, or the weight divided by w .

Proof. We prove by induction on n_l . Under the equal-weight assumption, we scale all the weights by $1/w$ so that the weight of each Pauli error is 1.

First, recall from Lemma 4 and Fig. 15 that for a single Z-type ancilla loss m , the possible detector patterns correspond to edges S_1, S_2, S_3 in the matching graph, which form a Z-shaped path, and for an X-type ancilla loss, there is only one possible edge S_4 that can be triggered.

Base case ($n_l = 1$): Consider a single loss event m with mismatch $L = \mathcal{D}_{m,j} \oplus \mathcal{D}_{m,k}$.

- Case 1: Adjacent segments.** L corresponds to the difference between adjacent segments, e.g., $L = S_1 \oplus S_2$ or $L = S_2 \oplus S_3$. In the matching graph, S_1 and S_2 (or S_2 and S_3) share a vertex, and their other endpoints are connected by a single Pauli error edge e of weight w (forming a triangle). Thus, L is homologous to e . Since $C_P \oplus L$ forms an undetectable logical error, $C_P \oplus e$ is an undetectable logical error, implying $|C_P \oplus e| \geq d$. By the reverse triangle inequality:

$$|C_P| \geq |C_P \oplus e| - |e| \geq d - 1. \quad (\text{C1})$$

Therefore $|C_P| \geq d - 1$.

- Case 2: Non-adjacent segments.** If $L = S_1 \oplus S_3$, then C_P must bridge the disjoint supports of S_1 and S_3 to form a cycle. The minimal bridge is S_2 (weight w), so $|C_P| \geq |C'_P| + 1$ with $C_P = C'_P \oplus S_2$. The error becomes $C_P \oplus L = C'_P \oplus (S_1 \oplus S_2 \oplus S_3)$. Since the term $S_1 \oplus S_2 \oplus S_3$ has endpoints with distance 2 on the matching graph, the condition $|C'_P \oplus (S_1 \oplus S_2 \oplus S_3)| \geq d - 2$ implies $|C'_P| \geq d - 2$, and thus $|C_P| \geq d - 1$.
- Case 3: One of $\mathcal{D}_{m,j}$ or $\mathcal{D}_{m,k}$ is empty.** In this case, $\mathcal{D}_{m,j} \oplus \mathcal{D}_{m,k}$ is a single edge of weight w . Following the analysis in Case 1, we obtain $|C_P| \geq d - 1$.

In all cases, $|C_P| \geq d - 1$.

Inductive case ($n_l > 1$): The statement follows by repeating the analysis from the base case for each of the n_l losses. As shown above, each loss mismatch (whether adjacent or non-adjacent) effectively reduces the required size of the Pauli component C_P by at most 1. Also, the construction of the Pauli envelope ensures linearity of the detector patterns. Thus, for a configuration with n_l losses to form an undetectable logical error, the Pauli component must satisfy $|C_P| \geq d - n_l$. This completes the induction. \square

3. Proof of Envelope-MLE decoder Achieves Optimal Distance

Theorem 2 (MLE Decoder Achieves Optimal Distance). *The Envelope-MLE decoder achieves optimal distance for the Mid-SWAP syndrome extraction. Specifically, the decoder correctly decodes whenever*

$$n_l + 2n_p < d, \quad (7)$$

where n_l is the number of atom losses, n_p is the number of Pauli errors, and d is the code distance.

Proof. Suppose the actual error pattern consists of n_l atom losses and n_p Pauli errors.

Define the error configuration C as the symmetric difference between the actual error and the decoder output:

$$C = (\text{Actual error}) \oplus (\text{Decoder output}). \quad (\text{C2})$$

The error configuration C decomposes into:

- *Pauli component C_P :* XOR of actual and decoded Pauli errors.
- *Loss component L :* For each loss, the XOR of actual and decoded detector patterns.

By the optimality of the Envelope-MLE decoder (Lemma 5), the decoder outputs Pauli weight at most $n_p w$. Thus, the Pauli component satisfies:

$$|C_P| \leq 2n_p. \quad (\text{C3})$$

For decoder failure, C must be a non-trivial undetectable logical error. Applying Lemma 7 with the n_l loss pattern mismatches in L , we obtain $|C_P| \geq d - n_l$, and therefore:

$$|C_P| \geq d - n_l. \quad (\text{C4})$$

Combining these bounds, decoder failure requires:

$$2n_p + n_l \geq d. \quad (\text{C5})$$

Therefore, the decoder succeeds when $2n_p + n_l < d$. This bound is tight: there exists a configuration of d losses (e.g., forming a chain across the lattice) that completely erases the logical information, making recovery impossible for any decoder. This proves the optimality of both the Envelope-MLE decoder and the Mid-SWAP syndrome extraction. \square

4. Proof of Failure Probability Threshold

Theorem 3 (Failure Probability Threshold). *For the Mid-SWAP syndrome extraction with code distance d , subject to independent atom loss with rate p_{loss} and background Pauli errors with rate p_{pauli} , the failure probability of the Envelope-MLE decoder satisfies:*

$$P_{\text{fail}} = O\left(p_{\text{th}}^{-d}(p_{\text{loss}}^{d/2} + p_{\text{pauli}}^{d/2})\right),$$

where $d_{\text{loss}} \sim d$ and $d_{\text{pauli}} \sim d/2$.

Proof. By [Theorem 2](#), decoder failure requires an undetectable logical error with n_l losses and n_p Pauli errors satisfying $\omega := 2n_p + n_l \geq d$.

We bound the failure probability by summing over all connected error configurations with effective weight $\omega \geq d$. Let $N(s)$ denote the number of connected subgraphs of size s in the lattice. Since each error triggers a constant number of detectors, let μ be the maximum number of errors that can trigger overlapping detectors with a fixed error, which is also a constant. We have $N(s) \leq C(d)\mu^s$ for a polynomial function $C(d)$ and a constant μ [\[36\]](#).

For a configuration with s errors containing k losses and $s - k$ Pauli errors, the effective weight is $\omega = k + 2(s - k) = 2s - k$, occurring with probability $p_{\text{loss}}^k p_{\text{pauli}}^{s-k}$.

Define $p := \max(p_{\text{loss}}, \sqrt{p_{\text{pauli}}})$. Then:

$$p_{\text{loss}}^k p_{\text{pauli}}^{s-k} \leq p^k (p^2)^{s-k} = p^{2s-k} = p^\omega.$$

Summing over configurations:

$$P_{\text{fail}} \leq \sum_{\omega=d}^{\infty} \sum_{s=\lceil \omega/2 \rceil}^{\omega} C(d)\mu^s \binom{s}{2s-\omega} p^\omega \quad (\text{C6})$$

$$\leq \sum_{\omega=d}^{\infty} \tilde{C}(d) \tilde{\mu}^\omega p^\omega, \quad (\text{C7})$$

where $\tilde{C}(d), \tilde{\mu}$ absorb the inner sum and account for the combinatorial factors.

For $p < p_{\text{th}} := 1/\tilde{\mu}$, this geometric series converges to the following:

$$P_{\text{fail}} \leq \frac{\tilde{C}(d)(\tilde{\mu}p)^d}{1 - \tilde{\mu}p} \quad (\text{C8})$$

$$= \frac{\tilde{C}(d)}{1 - \tilde{\mu}p} \left(\frac{p}{p_{\text{th}}}\right)^d \quad (\text{C9})$$

$$\leq \frac{\tilde{C}(d)}{1 - \tilde{\mu}p} \left(\frac{p_{\text{loss}}^d + p_{\text{pauli}}^{d/2}}{p_{\text{th}}^d}\right) \quad (\text{C10})$$

$$= O\left(p_{\text{th}}^{-d}(p_{\text{loss}}^d + p_{\text{pauli}}^{d/2})\right). \quad (\text{C11})$$

The third step follows from $p = \max(p_{\text{loss}}, \sqrt{p_{\text{pauli}}})$, which gives $p^d = \max(p_{\text{loss}}^d, p_{\text{pauli}}^{d/2})$. \square

5. Extension to Loss-Resolving Errors

Theorem 5 (Extension to Loss-Resolving Errors). *The Envelope-MLE decoder can be extended to handle loss-resolving errors. Suppose with probability $p_{\text{readout}} = p_{\text{loss}}$ an atom is detected as lost but is actually not lost, and with probability p_{loss} a lost atom is randomly assigned to 0 or 1 with equal probability. We modify the Envelope-MLE decoder as follows: instead of enforcing $\sum_j x_{m,j} = r_m$ when $r_m = 0$, we relax this constraint to $\sum_j x_{m,j} \leq 1$ and add a penalty term $w \sum_j x_{m,j}$ to the objective function. This modification ensures the same failure probability scaling as without loss-resolving errors:*

$$P_{\text{fail}} = O\left(p_{\text{th}}^{-d}(p_{\text{loss}}^d + p_{\text{pauli}}^{d/2})\right).$$

Proof. Loss-resolving errors fall into two categories:

False positives (loss detected but atom not actually lost): These do not require special treatment. When the decoder is told an atom was lost (but it wasn't), we can treat the atom as if it were lost just before measurement, and this case is already handled by the original decoder.

False negatives (atom lost but not detected): For false negatives, the key observation is that an undetected atom loss requires two independent events: (1) the atom is lost, and (2) the loss-resolving measurement fails to detect it. Therefore, the effective probability is p_{loss}^2 .

Notice that after adding the penalty term, an undetected atom loss has the same form as a Pauli error; by repeating the proof of [Lemma 7](#), we can show that the failure condition generalizes to $2n_p + n_l + 2n_f \geq d$, where n_f is the number of false negatives.

Following the proof structure of [Theorem 3](#), we can show that the failure probability scaling is unchanged:

$$P_{\text{fail}} = O\left(p_{\text{th}}^{-d}(p_{\text{loss}}^d + p_{\text{pauli}}^{d/2})\right). \quad \square$$

We did not use this extension in our numerical evaluation as it significantly increases MILP problem sizes.

Appendix D: Proofs from Envelope-Matching decoder Section

This section contains the detailed proofs of lemmas and theorems from the Envelope-Matching decoder section. For simplicity, we assume all baseline Pauli-edge weights satisfy $w_e = w$.

1. Proof of Failure Condition

We first establish the following property regarding the matching graph weights. Recall that in [Algorithm 2](#), we set each edge weight to w , and then for each edge affected by atom loss, we reduce its weight to $0.5w$ for space-like edges and $0.25w$ for time-like edges.

Lemma 8. *After the reweighting procedure in Algorithm 2, for any single atom loss event:*

1. *The induced detector pattern can be matched with total weight at most $0.5w$.*
2. *The weight of a logical observable in the matching graph is reduced by at most $0.5w$.*

Proof. The first property follows directly from Figs. 14a and 14c. The only case worth noting is $t = 1$ in Fig. 14a, where it is possible for four detectors to be triggered. In this case, the pattern can be matched with two weight- $0.25w$ time-like edges.

The second property can be proved by analyzing how many edges are used in the minimum-weight path, similar to the proof of Lemma 7.

1. If none of the three edges are used, the weight of the path is not reduced.
2. If one of the three edges is used, the weight of the path is reduced by at most $0.5w$.
3. If S_1 and S_2 are selected, then the path has the same weight if we replace S_1 and S_2 with S_4 ; this reduces to the case where none or one of the edges is used.
4. If S_1 and S_3 are selected, then S_2 has to be selected to make the path connected; this reduces to the case where S_1 and S_2 are both selected.

In all cases, the weight of the path is reduced by at most $0.5w$. \square

Lemma 6 (Failure Condition of Envelope-Matching decoder). *For the Envelope-Matching decoder, decoding failure in the presence of n_p Pauli errors and n_l atom losses requires*

$$2n_p + 1.5n_l \geq d. \quad (8)$$

Proof. The MWPM decoder predicts an error correction E^c such that $\text{Weight}(E^c) \leq \text{Weight}(E)$. The decoder fails when $E \oplus E^c$ forms an undetectable logical error.

Using Lemma 8, we derive the bounds:

1. By Property 1, each loss event contributes weight at most $0.5w$ to the error matching. Thus, for n_p Pauli errors and n_l losses:

$$\text{Weight}(E) \leq (n_p + 0.5n_l)w. \quad (D1)$$

2. By Property 2, each loss event reduces the logical distance by at most $0.5w$. Thus, the total weight of the logical cycle satisfies:

$$\text{Weight}(E) + \text{Weight}(E^c) \geq (d - 0.5n_l)w. \quad (D2)$$

Combining these bounds with the failure condition $2\text{Weight}(E) \geq \text{Weight}(E) + \text{Weight}(E^c)$:

$$2(n_p + 0.5n_l)w \geq (d - 0.5n_l)w. \quad (D3)$$

Simplifying yields the final condition:

$$2n_p + 1.5n_l \geq d. \quad (D4)$$

\square

2. Proof of Failure Probability of Envelope-Matching decoder

Theorem 4 (Failure Probability of Envelope-Matching decoder). *For the Mid-SWAP syndrome extraction with code distance d , subject to independent atom loss with rate p_{loss} and background Pauli errors with rate p_{pauli} , the failure probability of the Envelope-Matching decoder satisfies:*

$$P_{\text{fail}} = O\left(p_{\text{th}}^{-d}(p_{\text{loss}}^{d_{\text{loss}}} + p_{\text{pauli}}^{d_{\text{pauli}}})\right).$$

where $d_{\text{loss}} \sim 2d/3$ and $d_{\text{pauli}} \sim d/2$.

Proof. Similar to the proof of Theorem 3, we define the effective weight $\omega = 2n_p + 1.5n_l$. For an error configuration with n_p Pauli errors and n_l losses, the probability is $p_{\text{pauli}}^{n_p} p_{\text{loss}}^{n_l}$.

Define $p := \max(p_{\text{loss}}^{2/3}, \sqrt{p_{\text{pauli}}})$. Then:

$$p_{\text{pauli}}^{n_p} p_{\text{loss}}^{n_l} \leq (p^2)^{n_p} (p^{1.5})^{n_l} = p^{2n_p + 1.5n_l} = p^\omega. \quad (D5)$$

Following the same counting argument as in Theorem 3, we sum over all error configurations with weight $\omega \geq d$:

$$P_{\text{fail}} \leq \sum_{\omega=d}^{\infty} \tilde{C}(d) \tilde{\mu}^\omega p^\omega. \quad (D6)$$

For $p < p_{\text{th}} := 1/\tilde{\mu}$, the series converges and is dominated by the $\omega = d$ term:

$$P_{\text{fail}} = O(p_{\text{th}}^{-d} p^d) = O\left(p_{\text{th}}^{-d}(p_{\text{loss}}^{2d/3} + p_{\text{pauli}}^{d/2})\right). \quad (D7)$$

\square

3. Extension to Loss-Resolving Errors

Theorem 6 (Extension to Loss-Resolving Errors). *The decoder can be extended to handle loss-resolving errors by initializing time-like edges with weight $w_T = 0.5w$ instead of w . The decoder maintains:*

$$P_{\text{fail}} = O\left(p_{\text{th}}^{-d}(p_{\text{loss}}^{2d/3} + p_{\text{pauli}}^{d/2})\right).$$

Proof. The extension handles two types of loss-resolving errors:

False positives: Similar to the proof of [Theorem 5](#), this case is already handled by the original decoder.

False negatives (atom lost but not detected): With the modified initialization ($w_T = 0.5w$), an undetected loss induces a detector pattern. The key observation is:

- The total weight for matching this pattern is at most w , equivalent to a single Pauli error.
- With no atom lost, the weight of a logical error is still dw .
- For each detected loss, the weight of a logical error is reduced by at most $0.5w$.

Therefore, in the failure condition analysis, an undetected loss (n_f false negatives) contributes similarly to Pauli errors:

$$2(n_p + n_f) + 1.5n_l \geq d. \quad (\text{D8})$$

Since false negatives happen with probability p_{loss}^2 , and it requires $d/2$ false negatives to form a logical error, repeating the proof of [Theorem 3](#), we can show that this contributes a term that scales like $(p_{\text{loss}}^2)^{d/2}$, which is dominated by $p_{\text{loss}}^{2d/3}$.

Therefore, the failure probability remains:

$$P_{\text{fail}} = O\left(p_{\text{th}}^{-d}(p_{\text{loss}}^{2d/3} + p_{\text{pauli}}^{d/2})\right).$$

□

We did not use this extension in our numerical evaluation as it significantly reduces the threshold for Pauli errors.

Appendix E: Upper Bound on the Effective Distance

We analyze the upper bound on the effective distance for (1) the conventional matching decoder, (2) Average-MLE decoder and Marginal-Matching decoder, and (3) SWAP syndrome extraction by directly constructing undecodable error patterns.

1. Conventional matching decoder

A conventional matching decoder decodes as if only Pauli errors were present. However, this approach only achieves $d_{\text{loss}} \sim d/3$.

As shown in [Fig. 16a](#), if errors similar to those in [Fig. 14a](#) ($t = 2$) occur, the conventional decoder incorrectly interprets this pattern as a weight-2 error, leading to miscorrection.

If $d/3$ such errors occur, the decoder fails.

2. Average-MLE decoder and Marginal-Matching decoder

The Average-MLE decoder [\[14\]](#) constructs a detector error model by enumerating all possible single-loss patterns and combining them with the Pauli detector error model. However, this approach only achieves $d_{\text{loss}} \sim d/2$, as shown in [Fig. 16b](#).

When an ancilla qubit is lost, the Average-MLE decoder will reweight all the blue edges to a constant weight, while other edges scale like $-\log \frac{p_{\text{pauli}}}{1-p_{\text{pauli}}}$.

It is possible that the ancilla loss triggers no detector at all (this can happen with a constant probability). However, since the blue path has a weight that becomes negligible compared with other edges, the decoder will connect the two red detectors using this path, even when the detectors are actually caused by boundary Pauli errors.

If $d/2$ such errors occur, the decoder fails.

3. SWAP syndrome extraction

As shown in [Fig. 16c](#), when a qubit is lost, either the red paths or the blue path can produce the same detector flips, and these cases have the same probability. Therefore, there is no way to distinguish them.

If $d/2$ such errors occur, any decoder fails. These cases can actually happen as illustrated in [Fig. 14b](#) ($t = 1$ and $t = 2$).

Appendix F: Extension to Other CSS Codes

In this section, we discuss how to extend our analysis beyond surface codes to more general CSS codes.

To make the Mid-SWAP technique applicable, we assume the following structure for the CSS code. We believe these assumptions can be relaxed by using different alternating syndrome extraction orders in time.

Definition 4 (Structure of a CSS Code). *Let C be a CSS code with parameters $[[n, k, d]]$. Assume there are n_x X -stabilizers and n_z Z -stabilizers such that $n_x + n_z = n$. (In general, these stabilizers need not be independent; we assume this so that the Mid-SWAP technique can be applied.)*

Let each X -type stabilizer S_i^X act on data qubits $q_{i,1}^X, q_{i,2}^X, \dots, q_{i,m_i}^X$, and let each Z -type stabilizer S_j^Z act on data qubits $q_{j,1}^Z, q_{j,2}^Z, \dots, q_{j,m_j}^Z$.

We assume that all $q_{i,1}^X$ for all $i \in \{1, \dots, n_x\}$ and $q_{j,1}^Z$ for all $j \in \{1, \dots, n_z\}$ are distinct. In other words, there is a one-to-one correspondence between ancilla qubits and data qubits such that each data qubit appears as the first qubit in exactly one stabilizer.

When the context is clear, we drop the superscripts X and Z for simplicity.

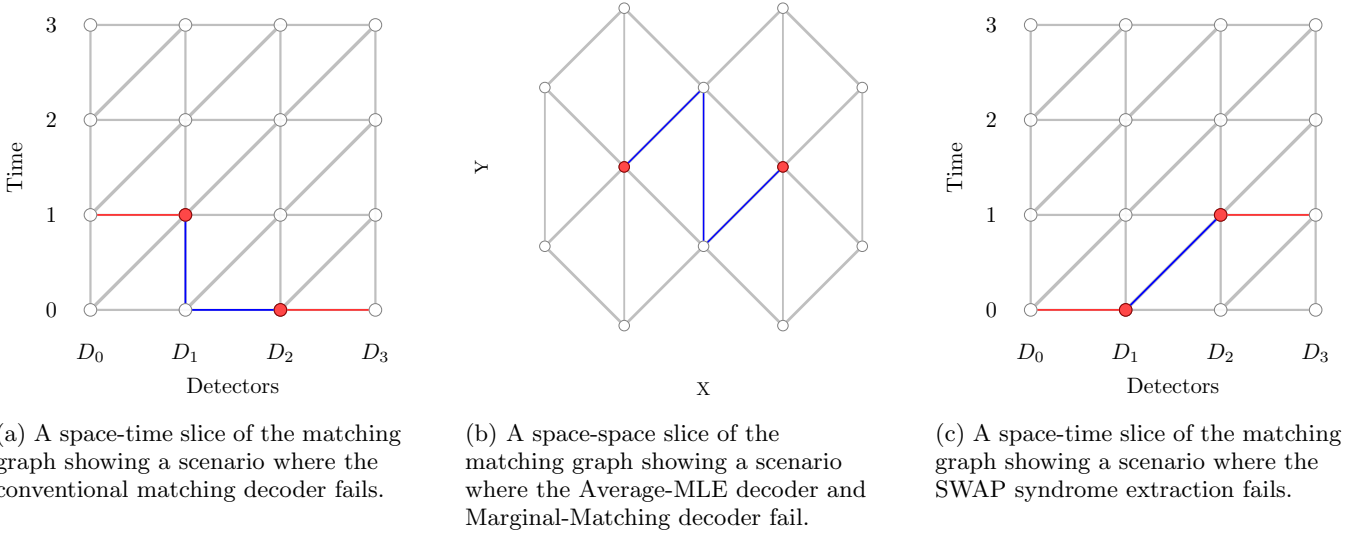


FIG. 16: Failure scenarios for (a) the conventional matching decoder, (b) the Average-MLE decoder and Marginal-Matching decoder, and (c) the SWAP syndrome extraction. Red dots represent detector flips. Red and blue edges represent two sets of edges with (asymptotically) equal weight that can produce the same detector flips, which cannot be distinguished by the decoder.

Definition 5 (Hook error). For each X -stabilizer S_i acting on data qubits $q_{i,1}, q_{i,2}, \dots, q_{i,m}$, we define a hook error $H_{i,t}$ as follows:

$$H_{i,t} = \prod_{j=1}^t X_{q_{i,j}}. \quad (\text{F1})$$

This describes how an X error on an X -ancilla a_i at time step t propagates to the data qubits. Note that the hook error $H_{i,t}$ has weight at most $m/2$ since we can always apply S_i to reduce its weight to an equivalent Pauli error.

We define the hook-error distance d_h of \mathcal{C} as the maximum number of hook errors and regular Pauli errors combined that can be tolerated by \mathcal{C} before inducing a nontrivial logical operator.

Formally, we have

$$\left(\prod_{i=1}^{n_h} H_{i,t_i} \right) \times \left(\prod_{i=1}^{n_p} X_{q_i} \right) \quad (\text{F2})$$

where any such product with $n_h + n_p < d_h$ does not implement a nontrivial logical operator. The hook-error distance for logical Z operators is defined similarly.

For any CSS code, we can construct a simple syndrome extraction circuit that uses only X -type and Z -type ancilla qubits to extract the syndrome with a circuit-level distance of d_h for Pauli errors.

Example 2. A syndrome extraction circuit can be constructed using the following steps:

1. Assign n_x X -type ancilla qubits to the X -type stabilizers, and n_z Z -type ancilla qubits to the Z -type stabilizers.

2. For each syndrome extraction cycle, we initialize X -type ancilla qubits in the $|+\rangle$ state and Z -type ancilla qubits in the $|0\rangle$ state.
3. For each X -type ancilla a_i associated with qubits $q_{i,1}, q_{i,2}, \dots, q_{i,m}$, apply $CNOT(a_i, q_{i,1}), CNOT(a_i, q_{i,2}), \dots, CNOT(a_i, q_{i,m})$.
4. For each Z -type ancilla a_i associated with qubits $q_{i,1}, q_{i,2}, \dots, q_{i,m}$, apply $CNOT(q_{i,1}, a_i), CNOT(q_{i,2}, a_i), \dots, CNOT(q_{i,m}, a_i)$.
5. Measure all the X -type ancilla qubits in the X -basis and all the Z -type ancilla qubits in the Z -basis.

Some examples of codes satisfying the condition $d_h = d$ include surface codes, hypergraph product (HGP) codes [37], and some bivariate bicycle (BB) codes [38]. For such codes, the syndrome extraction circuits are also optimal in terms of circuit-level distance [39, 40].

We can apply the Mid-SWAP technique to this syndrome extraction circuit to obtain a new syndrome extraction circuit with atom replenishment.

Example 3 (Mid-SWAP syndrome extraction circuit). Formally, for the third and fourth steps of [Example 2](#), we insert a SWAP gate between the ancilla-data qubit pair after the first $CNOT$ gate.

1. For each X -type ancilla a_i associated with qubits $q_{i,1}, q_{i,2}, \dots, q_{i,m}$, apply $CNOT(a_i, q_{i,1}), SWAP(a_i, q_{i,1}), CNOT(a_i, q_{i,2}), \dots, CNOT(a_i, q_{i,m})$.
2. For each Z -type ancilla a_i associated with qubits $q_{i,1}, q_{i,2}, \dots, q_{i,m}$, apply $CNOT(q_{i,1}, a_i),$

$$\begin{aligned} & \text{SWAP}(q_{i,1}, a_i), & \text{CNOT}(q_{i,2}, a_i), & \dots, \\ & \text{CNOT}(q_{i,m}, a_i). \end{aligned}$$

To analyze the tolerance to atom loss, we need to generalize the loss pattern of [Lemma 4](#) to this CSS setting.

Lemma 9 (Loss-induced hook error). *Let \mathcal{C} be the Mid-SWAP syndrome extraction circuit from [Example 3](#).*

Let a_i be an X -type ancilla associated with qubits $q_{i,1}, q_{i,2}, \dots, q_{i,m}$. If an atom loss of a_i is detected, then the Pauli envelope has the following form when propagated to the end of this syndrome extraction cycle:

$$E = \{I_{q_{i,1}}, Z_{q_{i,1}}\} \oplus \{H_{i,t}\}_{t=0}^m \oplus \{\text{Measurement errors}\}. \quad (\text{F3})$$

where $H_{i,t}$ is the hook error

$$H_{i,t} = \prod_{j=1}^t X_{q_{i,j}}. \quad (\text{F4})$$

The measurement errors are irrelevant to proving the circuit-level distance, so we ignore them from now on.

Furthermore, if a_i is a Z -type ancilla, it will only trigger a data error on $q_{i,1}$.

Proof. The construction of the Mid-SWAP syndrome extraction circuit ensures that each atom loss affects at most two consecutive syndrome extraction cycles. Thus, we only need to analyze two consecutive cycles and will focus on the remaining errors on the data qubits after these two cycles. Suppose the atom loss occurs at time step t (after the t -th CNOT gate) and is detected on the ancilla qubit a_i at the end of the second cycle.

1. $0 \leq t \leq m$: the atom is lost during the data phase. The Pauli envelope can be written as

$$E_i = \bigoplus_{\tau=t}^m E_{q_{i,1}}^\tau \oplus E_{a_i}^{m+1}, \quad (\text{F5})$$

where $E_q^\tau = \{I_q^\tau, X_q^\tau, Y_q^\tau, Z_q^\tau\}$ denotes the Pauli error set on qubit q at time step τ .

For any element in the first term of the Pauli envelope $\bigoplus_{\tau=t}^m E_{q_{i,1}}^\tau$, the residual error on the data qubit is an arbitrary Pauli error on $q_{i,1}$.

For the second term of the Pauli envelope $E_{a_i}^{m+1}$, this corresponds to an error on ancilla qubit a_i after the first CNOT gate in the second cycle; when propagated to the data qubits, it becomes an X error or identity.

Therefore, the joint effect of these two terms is an arbitrary Pauli error on data qubit $q_{i,1}$, which can be written in the form

$$E = \{I_{q_{i,1}}, Z_{q_{i,1}}\} \oplus \{H_{i,t}\}_{t=0}^1. \quad (\text{F6})$$

2. $m < t \leq 2m$: The Pauli envelope contains only a single Pauli operator:

$$E_i = E_{a_i}^t. \quad (\text{F7})$$

When this error propagates to the data qubits, it becomes an X -type hook error of the form

$$H_{i,t} = \prod_{j=1}^{t-m} X_{q_{i,j}}. \quad (\text{F8})$$

Therefore, $\{I_{q_{i,1}}, Z_{q_{i,1}}\} \oplus \{H_{i,t}\}_{t=0}^m$ is a valid Pauli envelope for the atom loss of a_i . \square

Without loss-resolving readouts, the effect of atom loss is similar to hook errors or single data-qubit errors. Thus, if a code can tolerate $\lfloor (d_h + 1)/2 \rfloor$ hook errors or single data-qubit errors, then it can also tolerate $\lfloor (d_h + 1)/2 \rfloor$ atom loss errors.

Theorem 7 (Tolerance to atom loss without loss-resolving readouts). *Even without loss-resolving readouts, the Mid-SWAP syndrome extraction circuit can correct $\lfloor (d_h + 1)/2 \rfloor$ atom loss errors.*

With loss-resolving readouts, the decoder obtains more information about the atom loss. The decoder ([Algorithm 1](#)) will know the index i of the hook error $H_{i,t}$ through the loss-resolving readouts but will be uncertain about the exact time step t . If the decoder guesses the time step as t^* , then the residual error is H_{i,t^*} .

We define a segment-hook error as an error on a contiguous segment of data qubits in the index order $q_{i,1}, q_{i,2}, \dots, q_{i,m}$ associated with stabilizer S_i^X . Formally, it is an error of the form

$$H_{i,j_1,j_2} = \prod_{j=j_1}^{j_2} X_{q_{i,j}}. \quad (\text{F9})$$

where $1 \leq j_1 \leq j_2 \leq m$, and contiguity means consecutive indices $j_1, j_1 + 1, \dots, j_2$ in this order.

Theorem 8 (Tolerance to atom loss with loss-resolving readouts). *If a code satisfies the condition that d_s segment-hook errors cannot implement a nontrivial logical operator, then it can correct d_s atom loss errors with loss-resolving readouts.*

Surface codes (as proved in this paper) satisfy the stronger condition $d_s = d_h = d$, thus achieving optimal tolerance to atom loss with the Mid-SWAP technique. The larger family of HGP codes, which are known to support efficient error correction [\[41–43\]](#), state preparation [\[44\]](#), and logical gates [\[45–57\]](#), have also been shown to achieve the condition $d_s = d_h = d$ [\[39, 40\]](#). Thus, they are strong candidates for quantum error-correcting codes for neutral-atom architectures.

Appendix G: Extension to Correlated Atom Loss

We now discuss the tolerance to correlated atom loss. A correlated atom loss is an error in which a physical CZ gate causes both atoms to be lost simultaneously.

Intuitively, correlated atom loss is more destructive than independent atom loss as it introduces high-weight errors easily. However, as we will see, correlated atom loss has the same effective distance as Pauli errors even without loss-resolving readouts.

Lemma 10 (Correlated loss-induced hook error). *Let \mathcal{C} be the Mid-SWAP syndrome extraction circuit from Example 3.*

Let a_i be an X -type ancilla associated with qubits $q_{i,1}, q_{i,2}, \dots, q_{i,m}$. If a correlated atom loss of a_i with some $q_{i,\tau}$ occurs, then the Pauli envelope of this particular loss configuration has the following form when propagated to the end of this syndrome extraction cycle:

$$E = \{I_{q_{i,\tau}}, Z_{q_{i,\tau}}\} \oplus \{H_{i,\tau}\} \oplus \{\text{Measurement errors}\}. \quad (\text{G1})$$

where $H_{i,\tau}$ is the hook error

$$H_{i,\tau} = \prod_{j=1}^{\tau} X_{q_{i,j}}. \quad (\text{G2})$$

Proof. The proof follows from the same argument as Lemma 9. \square

Theorem 9 (Tolerance to correlated atom loss without loss-resolving readouts). *Even without loss-resolving readouts, the circuit can tolerate $\lfloor (d_h + 1)/2 \rfloor$ correlated atom loss errors.*

With loss-resolving readouts, correlated atom loss provides more information about the locations of the lost atoms. For example, if only one pair of qubits is lost, in the Mid-SWAP circuit, one pair of qubits interacts only once, so we can perfectly identify the locations of the lost atoms. If perfectly identifying the location of the lost atoms were possible, the Pauli envelope contains only a single hook error, and the decoder can correctly decode n_h correlated atom loss errors, meaning $2n_h$ atoms are lost simultaneously.

Although perfectly identifying the location of the lost atoms is not always possible, we can still modify the Envelope-MLE decoder to handle correlated atom loss.

The high-level idea is to jointly minimize the number of correlated losses and independent loss events.

Algorithm 3 (Envelope-MLE decoder with correlated atom loss). *Before receiving the detector patterns, the decoder first performs the following steps as preprocessing:*

1. **Find the Pauli envelope for each loss-resolving readout:** For each loss-resolving readout r_m corresponding to a single atom loss, find its Pauli envelope E_m according to Lemma 2.

2. **Find the Pauli envelope for each correlated loss-resolving readout:** For each loss-resolving readout $r_m \oplus r_n$ corresponding to a single correlated atom loss, find its Pauli envelope $E_{m,n}$ according to Lemma 2.

3. **Assign variables for loss patterns:** For each pair $(\mathcal{D}_{m,j}, \mathcal{O}_{m,j}) \in \mathcal{S}(E_m, \emptyset)$, assign a binary variable $x_{m,j} \in \{0, 1\}$, indicating whether the loss pattern is selected ($x_{m,j} = 1$) or not ($x_{m,j} = 0$).

4. **Assign variables for correlated loss patterns:** For each pair $(\mathcal{D}_{(m,n),j}, \mathcal{O}_{(m,n),j}) \in \mathcal{S}(E_{m,n}, \emptyset)$, assign a binary variable $x_{(m,n),j} \in \{0, 1\}$, indicating whether the correlated loss pattern is selected ($x_{(m,n),j} = 1$) or not ($x_{(m,n),j} = 0$).

5. **Assign variables for Pauli errors:** For each Pauli error mechanism i in the circuit, assign a binary variable $y_i \in \{0, 1\}$, indicating whether the Pauli error mechanism is selected ($y_i = 1$) or not ($y_i = 0$).

After receiving the detector patterns, the decoder performs the following steps:

1. **Enforce constraints:**

(i) Detector satisfaction: For each detector d , enforce

$$\sum_i D_{i,d} y_i + \sum_{m,j} D_{m,j,d} x_{m,j} + \sum_{(m,n),j} D_{(m,n),j,d} x_{(m,n),j} \equiv s_d \pmod{2}, \quad (\text{G3})$$

where $D_{i,d} \in \{0, 1\}$ indicates whether Pauli error i flips detector d , $D_{m,j,d} \in \{0, 1\}$ indicates whether loss pattern (m, j) flips detector d , and $s_d \in \{0, 1\}$ is the observed detector value at index d .

(ii) Loss exclusivity: For each loss-resolving readout r_m , where $r_m = 1$ indicates the m -th atom is lost, enforce

$$\sum_j x_{m,j} + \sum_{(m,n),j} x_{(m,n),j} = r_m, \quad (\text{G4})$$

ensuring exactly one detector pattern is selected per loss event.

2. **Minimize loss error count and then Pauli error count:** Solve the MILP:

$$\min_{x,y} \left(\sum_{m,j} x_{m,j} + \sum_{(m,n),j} x_{(m,n),j} + \epsilon \sum_i w_i y_i \right) \quad (\text{G5})$$

subject to the above constraints, where ϵ is a small positive constant ensuring the loss error count is minimized first.

3. **Predict logical observable:** Let $x_{m,j}^*, y_i^*$ be the optimal solutions to the MILP. Calculate the predicted logical flip:

$$\mathcal{O}_{pred} = \bigoplus_i y_i^* \mathcal{O}_i \oplus \bigoplus_{m,j} x_{m,j}^* \mathcal{O}_{m,j} \oplus \bigoplus_{(m,n),j} x_{(m,n),j}^* \mathcal{O}_{(m,n),j} \quad (\text{G6})$$

where \mathcal{O}_i is the observable flip caused by Pauli error i .

For evaluation, we consider only atom loss after each *CNOT* gate and do not consider Pauli errors. For an error rate p and correlated loss contribution η , each atom has probability $p(1 - \eta)/2$ of being lost independently and probability $p\eta/2$ of being lost together with its partner. Thus, the marginal probability of each atom being lost remains $p/2$. As shown in Fig. 17, the threshold

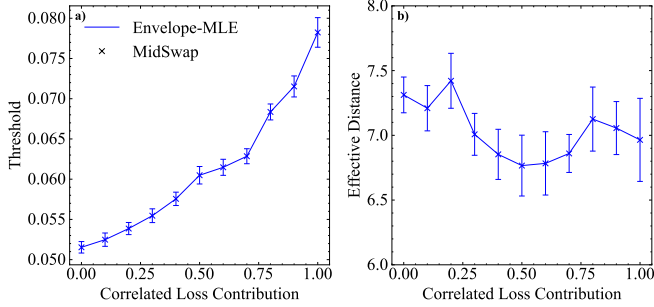


FIG. 17: (a) Threshold versus correlated-loss contribution; (b) effective distance at code distance 7 versus correlated-loss contribution.

increases from 0.05 to 0.08 as the correlated loss contribution η increases from 0 to 1. Furthermore, the effective distance remains approximately 7.

In summary, without loss-resolving readouts, both independent atom loss and correlated atom loss behave similarly to hook errors. With loss-resolving readouts, independent atom loss behaves similarly to a segment-hook error with known locations, while correlated atom loss performs at least as well as independent atom loss and provides a higher threshold by supplying more information about the locations of the lost atoms.

We leave for future work a careful analysis of the interplay among regular Pauli errors, independent atom loss, and correlated atom loss errors, as well as a threshold theorem and relaxation of the assumptions that each ancilla qubit is only associated with one data qubit under alternating syndrome extraction orders.

Appendix H: Teleportation-based Syndrome Extraction Circuit

Ref. [14] also proposes a teleportation-based syndrome extraction circuit, which can be viewed as a modification of the Steane error correction circuit. The circuit is

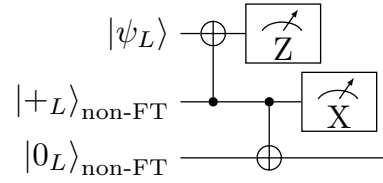


FIG. 18: Teleportation-based syndrome extraction circuit proposed in Ref. [14].

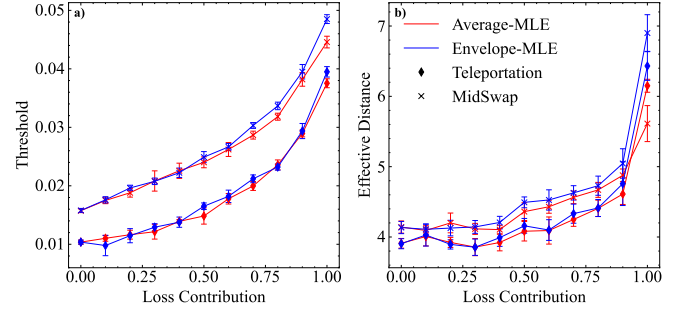


FIG. 19: Performance comparison between the teleportation circuit and the Mid-SWAP syndrome extraction: (a) threshold; (b) effective distance at code distance 7.

shown in Fig. 18. The two ancilla logical qubits are prepared non-fault-tolerantly, meaning that only one syndrome extraction round is performed. Although Ref. [14] shows that preparing the ancilla qubits fault-tolerantly can achieve a much higher threshold, this approach becomes a bottleneck when combined with transversal logical circuits. Therefore, we only consider the non-fault-tolerant preparation of ancilla qubits here, which takes constant time and provides full circuit-level distance.

We exclude the teleportation-based syndrome extraction circuit from the main text due to its significantly inferior performance compared to both Mid-SWAP syndrome extraction and SWAP syndrome extraction. The teleportation circuit exhibits two major disadvantages: (i) substantially lower threshold and effective distance, and (ii) considerably higher space-time overhead. Fig. 19 quantifies these performance gaps.

To ensure a fair comparison, we exclude idling errors from the teleportation circuit because its non-fault-tolerant state preparation is significantly affected by idling errors, while retaining the original error model for Mid-SWAP syndrome extraction.

The teleportation circuit achieves a threshold that is 0.5% to 1% lower than that of Mid-SWAP syndrome extraction, along with a slightly lower effective distance.

Appendix I: Measurement and reset error sensitivity

Both SWAP syndrome extraction and Mid-SWAP syndrome extraction exhibit different error-propagation

characteristics compared with the standard surface-code syndrome extraction circuit under pure Pauli noise. The standard surface-code circuit confines both measurement and reset errors to time-like edges, providing better tolerance to these errors. In contrast, SWAP syndrome extraction propagates measurement errors to space-like edges, while Mid-SWAP syndrome extraction propagates reset errors to space-like edges.

Fig. 20 examines how logical error rates depend on the relative magnitudes of reset and measurement error rates for both circuits. When the sum of reset and measurement error rates is fixed, the results reveal that the logical error rate of Mid-SWAP syndrome extraction increases as the reset error rate increases, whereas SWAP syndrome extraction’s logical error rate increases as the measurement error rate increases.

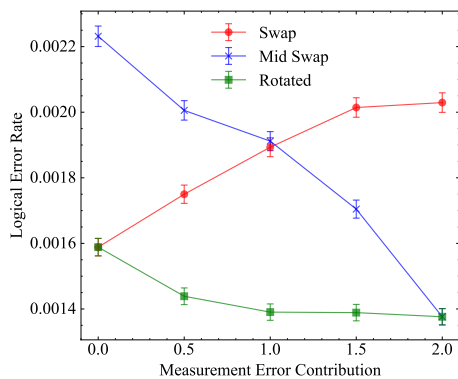


FIG. 20: Logical error rate behavior of Mid-SWAP syndrome extraction, SWAP syndrome extraction, and standard surface code syndrome extraction with varying reset and measurement error rates. Simulations are performed at distance $d = 5$ with error rate $p_{\text{pauli}} = p_{\text{loss}} = 0.008$. We scale the reset error rate to $0.008x$ and measurement error rate to $0.008(2 - x)$, where x ranges from 0 to 2. The Mid-SWAP syndrome extraction is more sensitive to reset errors, whereas the SWAP syndrome extraction is more sensitive to measurement errors.

Appendix J: Search for optimal hyperparameters

For Envelope-Matching decoder, our theoretical analysis derives reweighting coefficients of 0.5 for space-like edges and 0.25 for time-like edges.

With finite distances and error rates, these values might not give the best practical performance. Furthermore, any value in the range of $(0, 0.25)$ for time-like edges gives the same asymptotic performance.

Therefore, we view the reweighting coefficients as hyperparameters and empirically optimize them for the Envelope-Matching decoder in SWAP syndrome extraction and Mid-SWAP syndrome extraction and show the

result at code distance $d = 13$ as a function of loss contribution in Fig. 21.

The results show that the empirically optimized hyperparameters closely match the theoretical predictions for Mid-SWAP syndrome extraction, confirming the correctness of our analytical approach.

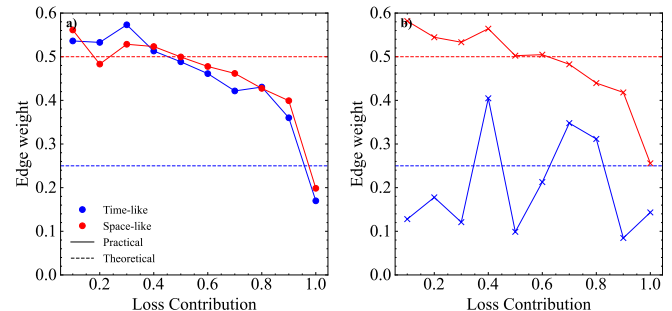


FIG. 21: Optimal hyperparameters for the Envelope-Matching decoder in (a) SWAP syndrome extraction and (b) Mid-SWAP syndrome extraction at code distance $d = 13$ as a function of the loss contribution. For Mid-SWAP syndrome extraction, the empirically optimized values closely match the theoretically predicted values of 0.5 for space-like edges and 0.25 for time-like edges, validating our analytical approach across different loss rates.

Appendix K: Nonlinearity of atom loss events

Our Envelope-MLE decoder (Algorithm 1) converts atom loss events to Pauli envelope errors rather than directly enumerating loss-induced detector-observable pairs as in Ref. [14]. This conversion is not only essential for our proof but also for the practical performance of the decoder.

Due to the nonlinearity of atom loss, when multiple losses occur simultaneously but are not modeled properly, the Envelope-MLE decoder has to use multiple Pauli errors to model the loss-induced errors, significantly degrading the performance.

Fig. 22 empirically validates this argument by comparing the Envelope-MLE decoder with the correct implementation and a modified version where the first step is removed, and the detector-observable pairs are enumerated by removing the Clifford gates affected by the loss. For SWAP syndrome extraction, the naive gate-removal approach yields significantly higher logical error rates, confirming that loss nonlinearity cannot be ignored in this circuit. However, for Mid-SWAP syndrome extraction, both approaches yield nearly identical performance, indicating that atom losses behave almost linearly in this architecture. We conjecture that this near-linearity also contributes to the superior performance of Mid-SWAP syndrome extraction over SWAP syndrome extraction when using Envelope-MLE decoder.

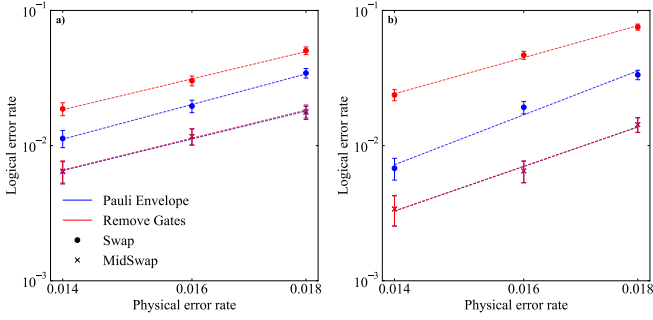


FIG. 22: Impact of the Pauli envelope on decoding performance for SWAP syndrome extraction and Mid-SWAP syndrome extraction at code distances (a) 5 and (b) 7. To emphasize the effect, we set the loss contribution to 1 in all cases.

Appendix L: Discussion on the practical scaling of Average-MLE decoder and Marginal-Matching decoder

Although we proved that both Average-MLE decoder and Marginal-Matching decoder can achieve $d_{\text{loss}} \sim d/2$ for the Mid-SWAP syndrome extraction and SWAP syndrome extraction, in actual experiments they scale more like $d_{\text{loss}} \sim 2d/3$.

This may be explained by the fact that we introduce alternating syndrome extraction orders in time to ensure replenishment of all boundary data qubits. This trick might also improve the effective distance as discussed by Gidney [58] and Lin et al. [59] although this is not why Ref. [14] and our evaluation use it.

We leave careful analysis of this phenomenon to future work.